



Phase transitions in self-gravitating systems and bacterial populations surrounding a central body

Pierre-Henri Chavanis , Julien Sopik, and Clément Sire 

Laboratoire de Physique Théorique, CNRS & Université de Toulouse–Paul Sabatier, France



(Received 9 August 2023; accepted 28 November 2023; published 16 January 2024)

We study the nature of phase transitions in a self-gravitating classical gas in the presence of a central body. The central body can mimic a black hole at the center of a galaxy or a rocky core (protoplanet) in the context of planetary formation. In the chemotaxis of bacterial populations, sharing formal analogies with self-gravitating systems, the central body can be a supply of “food” that attracts the bacteria (chemoattractant). We consider both microcanonical (fixed energy) and canonical (fixed temperature) descriptions and study the inequivalence of statistical ensembles. At high energies (respectively, high temperatures), the system is in a “gaseous” phase and at low energies (respectively, low temperatures) it is in a condensed phase with a “cusp-halo” structure, where the cusp corresponds to the rapid increase of the density of the gas at the contact with the central body. For a fixed density ρ_* of the central body, we show the existence of two critical points in the phase diagram, one in each ensemble, depending on the core radius R_* : for small radii $R_* < R_*^{\text{MCP}}$, there exist both microcanonical and canonical phase transitions (that are zeroth and first order); for intermediate radii $R_*^{\text{MCP}} < R_* < R_*^{\text{CCP}}$, only canonical phase transitions are present; and for large radii $R_* > R_*^{\text{CCP}}$, there is no phase transition at all. We study how the nature of these phase transitions changes as a function of the dimension of space. We also discuss the analogies and the differences with phase transitions in the self-gravitating Fermi gas [P. H. Chavanis, *Phys. Rev. E* **65**, 056123 (2002)].

DOI: [10.1103/PhysRevE.109.014118](https://doi.org/10.1103/PhysRevE.109.014118)

I. INTRODUCTION

Self-gravitating systems have a very peculiar thermodynamics due to the unshielded long-range attractive nature of the gravitational interaction [1–5]. Their study is interesting both from the viewpoint of astrophysics and statistical mechanics since a collection of N stars (composing globular clusters, galaxies...) constitutes a fundamental physical system with long-range interactions [6–8]. The subject started with the seminal paper of Antonov [9] who considered the thermodynamics of a self-gravitating classical gas confined within a spherical box of radius R . Since the system is isolated, it must be studied in the microcanonical ensemble. The box is necessary to prevent the evaporation of the gas and make the problem well-posed mathematically.¹ Following Ogorodnikov [13,14], Antonov studied the problem of maximizing the Boltzmann entropy at fixed mass and energy, and discovered that there is no global entropy maximum. There is

not even an extremum of entropy (canceling the first-order variations of entropy at fixed mass and energy) if the energy is below a critical value $E_c = -0.335GM^2/R$ [9]. Lynden-Bell and Wood [15] (see also Lynden-Bell [16]) interpreted this mathematical result in terms of a gravitational collapse that they called *gravothermal catastrophe*. Below the Antonov threshold $E < E_c$, the system takes a “core-halo” structure. The core, which has a negative specific heat, becomes hotter as it loses energy to the profit of the halo. Therefore, it continues to lose energy and evolves away from equilibrium. By this process, the system becomes hotter and hotter and more and more centrally condensed (as a consequence of the virial theorem). From thermodynamical arguments, the end-product of the gravothermal catastrophe is expected to be a *binary star* having a small mass ($2m \ll M$) but a huge binding energy [17]. The potential energy released by the binary star is redistributed in the halo in the form of kinetic energy (the system heats up) leading to an infinite (very large) entropy. Cohn [18] studied the dynamical evolution of the gravothermal catastrophe in the microcanonical ensemble (fixed energy) by numerically solving the orbit-averaged-Fokker-Planck equation [17,19]. He found that the collapse is self-similar and that the density profile develops a finite time singularity (core collapse). The central density becomes infinite in a finite time, scaling as $\rho \sim r^{-2.23}$, but the core mass $M_0(t) \sim (t_{\text{coll}} - t)^{0.41}$ tends to zero at the collapse time.² Therefore, the divergence of the central density is simply due to a *few* stars approaching

¹There is no statistical equilibrium state for a self-gravitating system in an infinite domain because the gas has the tendency to evaporate [10–12] (this is already the case for an ordinary gas if it is not confined within a container). In this sense, the strict statistical equilibrium state of a stellar system is made of two stars in Keplerian motion with all the other stars dispersed at infinity. Antonov [9] argued that the evaporation of stellar systems is a slow process so that, on intermediate timescales, everything happens as if the system were confined within a bounded container. In another interpretation, the box can mimic the effect of a tidal radius beyond which the particles are captured by a neighboring object (e.g., a galaxy in the vicinity of a globular cluster).

²Previously, Larson [20], Hachisu *et al.* [21], and Lynden-Bell and Eggleton [22] studied the same problem by using fluid equations and obtained similar results.

each other. In fact, a binary star is formed in the post-collapse regime and releases so much energy that the halo re-expands in a self-similar manner [23].³ Finally, a series of gravothermal oscillations follows [25]. On the other hand, at sufficiently high energies $E > E_c$, there exist statistical equilibrium states in the form of local entropy maxima at fixed mass and energy (there may also be saddle points of entropy but they are unstable) [9]. These states are metastable but they are very long lived because their lifetime scales like e^N (with $N \sim 10^6$ in a globular cluster) [26]. Therefore, these gaseous states can play an important role in the dynamics [27]. Indeed, most stellar systems like globular clusters are in the form of metastable gaseous states. They are described by the Michie-King model [28,29] which is a truncated Boltzmann distribution taking into account the evaporation of high energy stars. The thermodynamics of tidally truncated self-gravitating systems was studied by Katz [30] and Chavanis *et al.* [31]. In practice, a globular cluster relaxes through gravitational encounters toward a truncated equilibrium state. As it slowly evaporates, its central density increases (as a consequence of the virial theorem) and the cluster follows the King sequence with higher and higher central densities until a point at which it becomes unstable and undergoes core collapse as described above.

Since the statistical ensembles are not equivalent for self-gravitating systems (see Refs. [32,33] for early works on the subject and Refs. [1–5] for reviews), it can be of interest to study what happens when the system is in contact with a thermal bath imposing the temperature. In that case, the evolution of the system is dissipative and it must be studied in the canonical ensemble (CE). If one considers the problem of minimizing the free energy at fixed mass, then one finds that there is no global minimum of free energy. There is not even an extremum of free energy (canceling the first variations of free energy at fixed mass) below a critical temperature $T_c = GMm/2.52k_B R$ discovered by Emden [34]. The absence of a minimum of free energy leads to an *isothermal collapse* [35]. From statistical mechanics arguments, the end-product of this gravitational collapse is expected to be a *Dirac peak* containing all the mass since this structure has an infinite free energy. This has actually been proven rigorously by Kiessling [36]. Chavanis *et al.* [37,38] studied the dynamical evolution of the isothermal collapse for $T < T_c$ in the canonical ensemble (fixed temperature) by solving numerically and analytically the Smoluchowski-Poisson system describing a gas of self-gravitating Brownian particles in an overdamped limit. They found that the pre-collapse is self-similar and that the density profile develops a finite time singularity. The central density becomes infinite in a finite time, scaling as $\rho \sim r^{-2}$, but the core mass $M_0(t) \sim (t_{\text{coll}} - t)^{1/2}$ tends to zero at the collapse time. Therefore, “the central singularity contains no mass” in apparent contradiction with the thermodynamical expectation. In fact, the collapse continues after the singularity and a Dirac peak containing all the mass is finally formed in the post-collapse regime [39]. On the other hand, at sufficiently

high temperatures $T > T_c$, there exist statistical equilibrium states in the form of local free-energy minima at fixed mass (there may also be saddle points of free energy but they are unstable) [35]. These states are metastable but they are very long lived since their lifetime scales like e^N [26]. Therefore, these gaseous states can, again, play an important role in the dynamics. The self-gravitating Brownian gas may describe the evolution of planetesimals in the solar nebula in the context of planet formation. In that case, the particles experience a friction with the gas and a stochastic force due to Brownian motion or turbulence [40]. If the gas of particles is sufficiently dense (e.g., at special locations such as large-scale vortices), then self-gravity becomes important leading to gravitational collapse and planet formation.

The caloric curve of classical self-gravitating systems has the form of a spiral and the stability of the equilibrium states can be determined by using the Poincaré turning point criterion [15,41,42]. It is then found that the equilibrium states in the canonical ensemble become unstable after the first turning point of temperature T_c (corresponding to a density contrast of 32.1) while the equilibrium states in the microcanonical ensemble become unstable later, after the first turning point of energy E_c (corresponding to a density contrast of 709). Therefore, the statistical ensembles are inequivalent [15,32,33], which is a fundamental feature of systems with long-range interactions [8]. For classical self-gravitating systems, the region of ensemble inequivalence corresponds to a region of negative specific heats which is allowed (stable) in the microcanonical ensemble but forbidden (unstable) in the canonical ensemble.

Since the core collapse of classical point masses leads to a singularity (a binary star in the microcanonical ensemble or a Dirac peak in the canonical ensemble), some authors have studied what happens when a physical short-range regularization is introduced in the problem. In that case, we expect a phase transition between a gaseous (dilute) phase which is independent of the small-scale regularization and a condensed phase in which the small-scale regularization plays a prevalent role. Aronson and Hansen [43] considered the case of a self-gravitating hard-sphere gas in the canonical ensemble, modeled by a van der Waals equation of state, and evidenced a first-order canonical phase transition when the filling factor $\mu = R/R_*$ (where R is the system size and $R_* \sim N^{1/3}a$ is the radius of a compact object in which all the particles of size a are packed together) is sufficiently large. In the condensed phase, the equilibrium state has a “core-halo” structure with a dense solid core surrounded by a dilute atmosphere. Their study was followed by Stahl *et al.* [44] who used a more accurate equation of state and discussed interesting applications to planet formation. These authors considered both canonical and microcanonical ensembles and evidenced a first-order microcanonical phase transition in the case of very large filling factors. Instead of considering a classical hard-sphere gas, one can also consider a gas of self-gravitating fermions described by the Fermi-Dirac statistics. This system can have application in the context of white dwarf stars [45], neutron stars [46,47], and dark matter halos made of massive neutrinos [48–54]. In that case, the Pauli exclusion principle creates an “effective” repulsion between the particles and plays a role similar to that played by the core radius of

³Heggie and Stevenson [24] confirmed these results by constructing self-similar solutions of the orbit-averaged-Fokker-Planck equation in the pre-collapse and post-collapse regimes.

classical particles in a hard sphere gas.⁴ For self-gravitating fermions, the end-product of the collapse is a “core-halo” structure with a degenerate core (equivalent to a polytrope of index $n = 3/2$) surrounded by a dilute atmosphere. In the context of dark matter halos, the quantum core is called a “fermion ball.” The statistical mechanics of self-gravitating fermions was first considered by Hertel and Thirring [57] who showed rigorously (in a mathematical sense) that the mean-field approximation is exact in a proper thermodynamic limit. In another paper, Hertel and Thirring [58], and later Bilic and Viollier [59], discussed first-order canonical phase transitions in the self-gravitating Fermi gas but did not evidence first-order microcanonical phase transitions in their study. Chavanis [60] performed an exhaustive study of phase transitions in the self-gravitating Fermi gas in both canonical and microcanonical ensembles and explored the whole range of parameters. He showed the existence of two critical points, one in each ensemble. The control parameter can be written as $\mu = 17.2587(R/R_*)^{3/2}$, where R is the system size and $R_* = 0.181433 \hbar^2 / (Gm^{8/3} g^{2/3} M^{1/3})$ is the radius of a completely degenerate object of mass M at $T = 0$ (“white dwarf”) determined by the Planck constant \hbar [5]. Since R_* is fixed by quantum mechanics (for a given mass M), the control parameter measures the size of the system R . For large systems ($\mu > \mu_{\text{MCP}} \simeq 2670$), there exist both microcanonical and canonical phase transitions (of zeroth and first order), for systems of intermediate size ($\mu_{\text{CCP}} < \mu < \mu_{\text{MCP}}$) only canonical phase transitions exist, and for small systems ($\mu < \mu_{\text{CCP}} \simeq 83$) there is no phase transition at all. Other types of small-scale regularization have been introduced and lead to a similar phenomenology [61–65]. A review of phase transitions in self-gravitating systems is given in Ref. [5]. These results have been extended to self-gravitating fermions in general relativity [66–69]. They have also been discussed in the context of the fermionic King model (avoiding the artificial box) in Newtonian gravity [70] and general relativity [71].

In the present work, we study the nature of phase transitions in a self-gravitating classical gas of pointlike particles in the presence of a central body. The central body could mimic the effect of a black hole at the center of a galaxy or at the center of a globular cluster. It could also represent a rocky core (protoplanet) at the center of a giant gaseous planet like Jupiter or Saturn. The central body prevents the formation of singularities resulting from gravitational collapse and plays a role similar to that of a short-range regularization. There exists an equilibrium state for all accessible values of energy and temperature but canonical and microcanonical phase transitions can take place between a gaseous phase and a condensed phase. The condensed phase has the structure of a giant gaseous planet with a solid core surrounded by an atmosphere.⁵ The atmosphere has a “cusp-halo” structure, where the cusp corresponds to the rapid increase of the density of the gas at the contact with the central body. For a fixed density

ρ_* of the central body (and a fixed system size R), we show the existence of two critical points in the phase diagram, one in each ensemble, depending on the core radius R_* . For small radii $R_* < R_*^{\text{MCP}}$, there exist both microcanonical and canonical phase transitions (that are zeroth and first order). For intermediate radii $R_*^{\text{MCP}} < R_* < R_*^{\text{CCP}}$, only canonical phase transitions are present. Finally, for large radii $R_* > R_*^{\text{CCP}}$, there is no phase transition at all.⁶ This is qualitatively similar to the results previously obtained for self-gravitating fermions [5]. We also study how the canonical and microcanonical critical points R_*^{CCP} and R_*^{MCP} depend on the density of the central body ρ_* .

Our results can have applications for the problem of chemotaxis in biology [72,73]. Indeed, there exists a remarkable analogy between self-gravitating systems and bacterial populations [74]. In this analogy, the density of the gas $\rho(\mathbf{r}, t)$ is the counterpart of the density of bacteria $\rho(\mathbf{r}, t)$, and minus the gravitational potential $-\Phi(\mathbf{r}, t)$ is the counterpart of the concentration $c(\mathbf{r}, t)$ of the chemical (“pheromone”) produced by the bacteria (see Appendix A). As a result, the counterpart of a central mass M_* (black hole, protoplanet,...) giving rise to an external gravitational force $-\nabla\Phi_{\text{ext}}$ is a supply of “food” (chemoattractant) giving rise to a chemical drift $\nabla c_{\text{ext}}(\mathbf{r})$. Therefore, our study can have applications in biology up to a straightforward change of notations.

In this article, we will use the notations of astrophysics to make the connection with previous studies. We will essentially consider the spatial dimension $d = 3$ which is the most relevant dimension in astrophysics, and which leads to the richest variety of phase transitions. It corresponds to spherical halos and stars [45]. However, the dimension $d = 2$ corresponding to cosmic filaments [75,76] and the dimension $d = 1$ corresponding to sheets or pancakes [77,78] have also been considered in astrophysics and thermodynamics [1,38,79–84]. On the other hand, the dimension $d = 2$ is particularly relevant in biology [85] since cells of bacteria can be cultured on a petri dish. We will therefore study how the nature of phase transitions changes as a function of the dimension of space. A similar study of the effect of the dimension of space on the nature of gravitational phase transitions has been performed in Ref. [38] for classical self-gravitating systems, in Refs. [86–89] for self-gravitating fermions and bosons, and in Refs. [55,56] for particles with an exclusion constraint in position space.

The paper is organized as follows. In Sec. II we derive the basic equations determining the equilibrium structure of a self-gravitating isothermal gas around a central body. In Sec. III we plot the caloric curves of this self-gravitating gas in $d = 3$ dimensions and study the corresponding phase transitions. In Sec. IV we briefly consider the case of the dimensions $d = 1$ and $d = 2$. The Appendices regroup useful formulas that are needed in the theoretical part of the paper.

⁴One can also consider a Fermi-Dirac distribution in configuration space leading to qualitatively similar results [55,56].

⁵It can also describe the structure of a star cluster (galactic nucleus, globular cluster...) harboring a central black hole.

⁶One could equivalently fix the radius of the central body and increase the system size.

II. EQUILIBRIUM STRUCTURE OF A SELF-GRAVITATING ISOTHERMAL GAS AROUND A CENTRAL BODY

A. The maximum entropy principle

We consider a system of N pointlike particles of mass m interacting via Newtonian gravity in a space of dimension d . We allow for the presence of a spherically symmetric central body of mass M_* and radius R_* . This central body may mimic a black hole at the center of a galaxy or at the center of a globular cluster. It may also describe a rocky core surrounded by a gas (atmosphere) in the context of planet formation. The particles are enclosed within a spherical box of radius R to prevent the evaporation of the gas and make a statistical equilibrium state well-defined.⁷ Physically, a gas is never completely isolated from the surrounding. Therefore, the box can play the role of a tidal radius in the case of globular clusters and dark matter halos⁸ or represent the Hill sphere in the context of planet formation. The Hamiltonian of the self-gravitating system is

$$H = \sum_i \frac{1}{2} m v_i^2 + m^2 \sum_{i < j} u(|\mathbf{r}_i - \mathbf{r}_j|) + m \sum_i \Phi_{\text{ext}}(\mathbf{r}_i), \quad (1)$$

where $i = 1, \dots, N$ runs over the particles of the gas. The first term is the kinetic energy, the second term represents the interaction energy of the particles of the gas and the third term takes into account the interaction between the gas and the central body. The gravitational potential of interaction in d dimensions is given by

$$u(|\mathbf{r} - \mathbf{r}'|) = -\frac{1}{d-2} \frac{G}{|\mathbf{r} - \mathbf{r}'|^{d-2}} \quad (d \neq 2), \quad (2)$$

$$u(|\mathbf{r} - \mathbf{r}'|) = G \ln \frac{|\mathbf{r} - \mathbf{r}'|}{R} \quad (d = 2). \quad (3)$$

We treat the influence of the central body as an external potential (see Appendix B):

$$\Phi_{\text{ext}}(\mathbf{r}) = -\frac{1}{d-2} \frac{GM_*}{r^{d-2}} \quad (d \neq 2), \quad (4)$$

$$\Phi_{\text{ext}}(\mathbf{r}) = GM_* \ln \left(\frac{r}{R} \right) \quad (d = 2). \quad (5)$$

Let $f(\mathbf{r}, \mathbf{v})$ denote the distribution function of the system, i.e., $f(\mathbf{r}, \mathbf{v}) d\mathbf{r} d\mathbf{v}$ gives the mass of the particles of the gas whose position and velocity are in the cell $(\mathbf{r}, \mathbf{v}; \mathbf{r} + d\mathbf{r}, \mathbf{v} + d\mathbf{v})$. The integral of f over the velocity determines the spatial density $\rho = \int f d\mathbf{v}$. The total mass of the gas is

$$M = \int \rho d\mathbf{r}. \quad (6)$$

⁷In $d = 3$ dimensions, there is no statistical equilibrium state in an infinite domain (there are not even extrema of entropy at fixed mass and energy with a finite mass). In $d = 1$ and $d = 2$ dimensions, there exist statistical equilibrium states in an infinite domain that are studied analytically in a companion paper [90]. In the present paper, we shall only consider systems enclosed within a box of size R .

⁸An alternative to the box would be to consider a truncated Michie-King model [28,29] like in Refs. [30,31,70].

The spatial integral extends only in the region surrounding the central body, i.e., in the region $R_* < r < R$ covered by the gas. We consider a proper thermodynamic limit $N \rightarrow +\infty$ for self-gravitating systems in such a way that the rescaled energy and the rescaled temperature

$$\Lambda = -\frac{ER^{d-2}}{GM^2}, \quad \eta = \frac{\beta GMm}{R^{d-2}}, \quad (7)$$

are independent on N . We also introduce the parameters

$$\mu = \frac{M_*}{M}, \quad \zeta = \frac{R_*}{R}, \quad (8)$$

which represent the normalized mass and the normalized radius of the central body. In the $N \rightarrow +\infty$ limit,⁹ the mean-field approximation is exact, except close to a critical point [1–8]. Therefore, ignoring the correlations between the particles of the gas, the total energy of the system can be expressed as

$$E = \frac{1}{2} \int f v^2 d\mathbf{r} d\mathbf{v} + \frac{1}{2} \int \rho \Phi d\mathbf{r} + \int \rho \Phi_{\text{ext}} d\mathbf{r}, \quad (9)$$

where $\Phi_{\text{ext}}(\mathbf{r})$ is the potential created by the central body and $\Phi(\mathbf{r})$ is the gravitational potential created by the gas (see Appendix B). For $R_* \leq r \leq R$, they are respectively the solutions of the Laplace equation

$$\Delta \Phi_{\text{ext}} = 0, \quad (10)$$

and the Poisson equation

$$\Delta \Phi = S_d G \rho, \quad (11)$$

where $S_d = 2\pi^{d/2}/\Gamma(d/2)$ is the surface of a unit sphere in d dimensions. The energy $E = E_{\text{kin}} + W_{\text{tot}}$ of the gas is the sum of its kinetic energy $E_{\text{kin}} = (1/2) \int f v^2 d\mathbf{r} d\mathbf{v}$ and its total potential energy $W_{\text{tot}} = W + W_{\text{ext}}$, where $W = (1/2) \int \rho \Phi d\mathbf{r}$ is the self-gravitating energy of the gas and $W_{\text{ext}} = \int \rho \Phi_{\text{ext}} d\mathbf{r}$ is the gravitational energy of the gas in the potential created by the central body (see Appendix B).

For isolated Hamiltonian systems, the mass and the energy are conserved and the thermodynamical potential is the Boltzmann entropy¹⁰

$$S_B = -k_B \int \frac{f}{m} \ln \frac{f}{m} d\mathbf{r} d\mathbf{v}. \quad (12)$$

The Boltzmann entropy $S_B = k_B \ln \mathcal{W}$ measures the “disorder” of the system. It is proportional to the logarithm of the number $\mathcal{W}(\{n_i\})$ of *microstates* corresponding to a given *macrostate* [92]. At statistical equilibrium, the system is in the most mixed state consistent with all the constraints of the dynamics. Therefore, if the system is isolated, then the equilibrium state maximizes the Boltzmann entropy S_B at fixed mass M and energy E (microcanonical description). We thus

⁹A relevant scaling is $N \rightarrow +\infty$ with $m \sim 1/N$, $R \sim 1$, $G \sim 1$, $E \sim 1$ and $T \sim 1/N$ (see Appendix A in Ref. [91]).

¹⁰The entropy is defined up to an additive constant (not important in our case), which explains why the argument of the logarithm is not dimensionless.

have to solve the maximization problem

$$\max_f \{S_B[f] \mid E[f] = E, \quad M[f] = M\}. \quad (13)$$

Alternatively, if the system is in contact with a heat bath imposing the temperature T , then only the mass is conserved and the thermodynamical potential is the Boltzmann free energy $F_B = E - TS_B$. It is often more convenient to work with the Massieu function

$$J_B = \frac{S_B}{k_B} - \beta E, \quad (14)$$

where $\beta = 1/(k_B T)$ is the inverse temperature. The Massieu function is the Legendre transform of the entropy with respect to the energy. If the system is in contact with a heat bath, then the equilibrium state maximizes the Massieu function J at fixed mass M (canonical description). We thus have to solve the maximization problem

$$\max_f \{J_B[f] \mid M[f] = M\}. \quad (15)$$

The microcanonical ensemble is the proper description for (isolated) Hamiltonian systems and the canonical ensemble is the proper description for (dissipative) Brownian systems [5].

The extrema of entropy at fixed mass and energy (canceling the first-order variations of entropy under constraints) are determined by the variational principle

$$\frac{\delta S_B}{k_B} - \beta \delta E - \alpha_0 \delta M = 0, \quad (16)$$

where β and α_0 are Lagrange multipliers associated with the conservation of E and M . The extrema of Massieu function at fixed mass (canceling the first-order variations of Massieu function under constraints) are determined by the variational principle

$$\delta J_B - \alpha_0 \delta M = 0, \quad (17)$$

where α_0 is a Lagrange multiplier associated with the conservation of M . Using the identities

$$\delta S_B = -k_B \int \frac{\delta f}{m} \left(\ln \frac{f}{m} + 1 \right) d\mathbf{r} d\mathbf{v}, \quad (18)$$

$$\delta E = \frac{1}{2} \int \delta f v^2 d\mathbf{r} d\mathbf{v} + \int \Phi \delta \rho d\mathbf{r} + \int \Phi_{\text{ext}} \delta \rho d\mathbf{r}, \quad (19)$$

$$\delta M = \int \delta f d\mathbf{r} d\mathbf{v}, \quad (20)$$

we find that the variational principles (16) and (17) lead to the mean-field Maxwell-Boltzmann distribution

$$f = A' e^{-\beta m [v^2/2 + \Phi(\mathbf{r}) + \Phi_{\text{ext}}(\mathbf{r})]}, \quad (21)$$

where $A' = m e^{-\alpha_0 m - 1}$. Introducing the local (kinetic) pressure $P(\mathbf{r}) = \frac{1}{d} \int f v^2 d\mathbf{v}$ (see Appendix C), we find that the barotropic equation of state corresponding to the distribution (21) is that of an isothermal gas

$$P(\mathbf{r}) = \rho(\mathbf{r}) \frac{k_B T}{m}. \quad (22)$$

As a result, the velocity dispersion $\langle v^2 \rangle = dP/\rho = dk_B T/m$ is constant. Integrating Eq. (21) over the velocity, we find that

the spatial density is the mean-field Boltzmann distribution

$$\rho = A e^{-\beta m [\Phi(\mathbf{r}) + \Phi_{\text{ext}}(\mathbf{r})]}, \quad (23)$$

where $A = (2\pi/\beta m)^{d/2} A'$. Therefore, combining Eqs. (11) and (23), the structure of the gas around the central body is obtained by solving the Boltzmann-Poisson equation

$$\Delta \Phi = S_d G A e^{-\beta m (\Phi + \Phi_{\text{ext}})}, \quad (24)$$

with appropriate boundary conditions (see below), and by relating the Lagrange multipliers to the constraints. We can then plot the series of equilibria $\beta(E)$ for given values of M_* and R_* (or in dimensionless form $\eta(\Lambda)$ for given μ and ζ). The control parameter is E in the microcanonical ensemble and β in the canonical ensemble. The stable region of the series of equilibria defines the caloric curve in the considered ensemble. Note that the extrema (regarding the first variations) of the entropy S_B at fixed E and M , and the extrema of the Massieu function J_B at fixed T and M are the same, and both determine a self-gravitating isothermal gas. However, the stability of the gas (regarding the second variations of S_B or J_B with appropriate constraints) may differ in the microcanonical (fixed E) and canonical (fixed T) ensembles. When this happens, this is referred to a situation of *ensemble inequivalence*. It can be shown that canonical stability [Eq. (15)] implies microcanonical stability [Eq. (13)], but the converse is in general false for systems with long-range interactions [93,94]. For example, negative specific heats are forbidden in the canonical ensemble while they are allowed in the microcanonical ensemble. Therefore, canonical stability only provides a *sufficient* condition of microcanonical stability. Ensemble inequivalence and phase transitions in self-gravitating systems is well-documented in the absence of a central body [1–5]. We shall study how the presence of a central body affects these results.

B. The Emden equation

Introducing the total gravitational potential

$$\Phi_{\text{tot}} = \Phi + \Phi_{\text{ext}}, \quad (25)$$

and using Eq. (10), we can rewrite the Boltzmann-Poisson equation (24) as

$$\Delta \Phi_{\text{tot}} = S_d G A e^{-\beta m \Phi_{\text{tot}}}. \quad (26)$$

It can be shown that the maximum entropy state of a nonrotating self-gravitating system is spherically symmetric [9].¹¹ In that case, we can rewrite the foregoing equation as

$$\frac{1}{r^{d-1}} \frac{d}{dr} \left(r^{d-1} \frac{d\Phi_{\text{tot}}}{dr} \right) = S_d G A e^{-\beta m \Phi_{\text{tot}}}. \quad (27)$$

¹¹This result is valid for a self-gravitating system without central body. In the presence of a central body that creates an excluded region for the self-gravitating system, we can wonder if there can be a symmetry-breaking phase transition toward an equilibrium state that is not spherically symmetric and if this state can be (meta)stable. This interesting possibility will not be considered in the present paper.

It has to be solved with the boundary condition

$$\frac{d\Phi_{\text{tot}}}{dr}(R_*) = \frac{d\Phi_{\text{ext}}}{dr}(R_*) = \frac{GM_*}{R_*^{d-1}}, \quad (28)$$

resulting from Eq. (B2) and the fact that $d\Phi/dr(R_*) = 0$, since $\rho = 0$ for $r \leq R_*$ (see Appendix D). Multiplying Eq. (27) by r^{d-1} , integrating between R_* and r , and using the boundary condition (28), we obtain the integrodifferential equation

$$r^{d-1} \frac{d\Phi_{\text{tot}}}{dr} = GM_* + GA \int_{R_*}^r e^{-\beta m \Phi_{\text{tot}}(r')} S_d r'^{d-1} dr'. \quad (29)$$

This equation can also be written as

$$\frac{d\Phi_{\text{tot}}}{dr} = \frac{GM_{\text{tot}}(r)}{r^{d-1}}, \quad (30)$$

where

$$M_{\text{tot}}(r) = M_* + M(r) = M_* + \int_{R_*}^r \rho(r') S_d r'^{d-1} dr' \quad (31)$$

is the total mass contained within the sphere of radius r . This is Newton's law in d dimensions (see Appendix D).

To determine the structure of the isothermal gas, we introduce the function

$$\psi = \beta m (\Phi_{\text{tot}} - \Phi_{\text{tot},0}), \quad (32)$$

where $\Phi_{\text{tot},0} = \Phi_{\text{tot}}(R_*)$ is the total gravitational potential at $r = R_*$. Then, the density can be written as

$$\rho = \rho_0 e^{-\psi}, \quad (33)$$

where $\rho_0 = \rho(R_*)$ is the density of the gas at the contact with the central body. By an abuse of language, ρ_0 will be called the central density and $\Phi_{\text{tot},0}$ will be called the central total gravitational potential. Introducing the dimensionless radius

$$\xi = (S_d G \beta m \rho_0)^{1/2} r, \quad (34)$$

the Boltzmann-Poisson equation (27) reduces to the form

$$\frac{1}{\xi^{d-1}} \frac{d}{d\xi} \left(\xi^{d-1} \frac{d\psi}{d\xi} \right) = e^{-\psi}, \quad (35)$$

which is called the Emden equation [34,45]. In the presence of a central body, this equation has to be solved with the boundary conditions [see Eq. (28)]

$$\psi(\xi_0) = 0, \quad \psi'(\xi_0) = \frac{\eta_0}{\xi_0}, \quad (36)$$

where we have defined

$$\xi_0 = (S_d G \beta m \rho_0)^{1/2} R_*, \quad \eta_0 = \beta G M_* m / R_*^{d-2}. \quad (37)$$

In the absence of a central body, the boundary conditions are replaced by $\psi(0) = \psi'(0) = 0$ [34,45]. The Emden equation (35) can also be written in the form of an integrodifferential equation [see Eq. (29)]

$$\xi^{d-1} \frac{d\psi}{d\xi} = \eta_0 \xi_0^{d-2} + \int_{\xi_0}^{\xi} e^{-\psi(\xi')} \xi'^{d-1} d\xi'. \quad (38)$$

The Emden equation (35) must be solved numerically (see Fig. 1). We can however easily determine the asymptotic

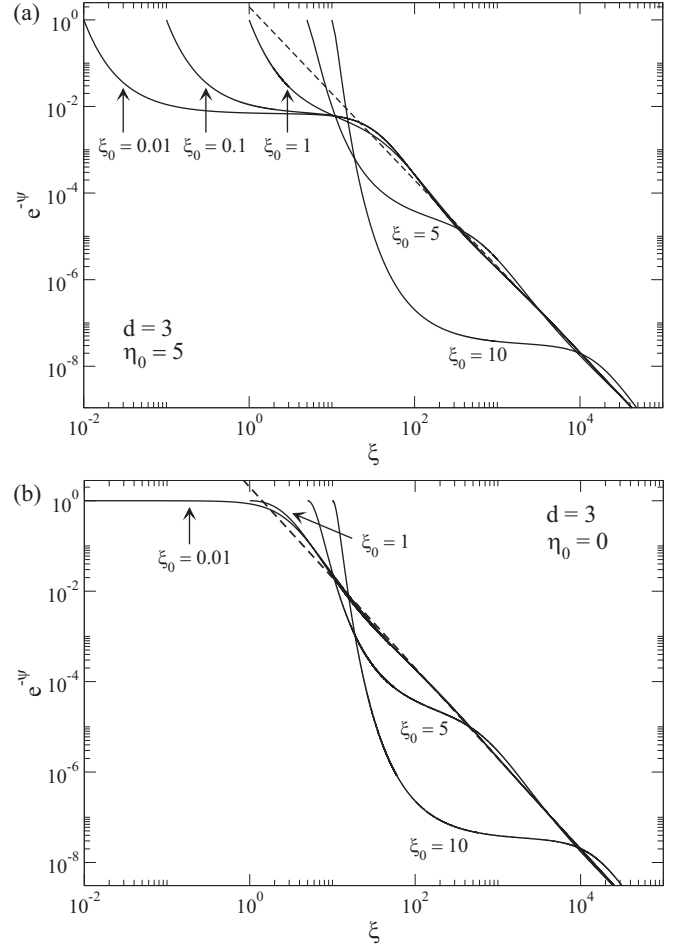


FIG. 1. Dimensionless density profile $e^{-\psi}$ that is the solution of the Emden equation with a central body in $d = 3$ dimensions. We have selected $\eta_0 = 5$ and $\eta_0 = 0$ (hole) for illustration.

behaviors of the solutions. For $\xi \rightarrow \xi_0$, we can expand the solution in Taylor series and we find that

$$\begin{aligned} \psi(\xi) = & \frac{\eta_0}{\xi_0} (\xi - \xi_0) + \frac{1}{2} \left[1 - \frac{(d-1)\eta_0}{\xi_0^2} \right] (\xi - \xi_0)^2 \\ & + \frac{1}{6} \left[\frac{1-d-\eta_0}{\xi_0} + \frac{d(d-1)\eta_0}{\xi_0^3} \right] (\xi - \xi_0)^3 \\ & - \frac{1}{24} \left[1 + \frac{1-d^2-2(d-1)\eta_0-\eta_0^2}{\xi_0^2} \right. \\ & \left. + \frac{(d-2)(d-1)^2\eta_0}{\xi_0^4} \right] (\xi - \xi_0)^4 + O[(\xi - \xi_0)^5]. \end{aligned} \quad (39)$$

Therefore, when $\eta_0 \neq 0$ and $\xi_0 \neq 0$, the density profile of the gas close to the central body behaves as

$$\rho \sim \rho_0 e^{-\frac{\eta_0}{\xi_0}(\xi - \xi_0)} \quad (\xi \rightarrow \xi_0). \quad (40)$$

It presents a spike which is clearly visible in Fig. 1(a). By contrast, when $\eta_0 = 0$ and $\xi_0 \neq 0$ (hole), the density profile of the gas close to the central body behaves as

$$\rho \sim \rho_0 e^{-\frac{1}{2}(\xi - \xi_0)^2} \quad (\xi \rightarrow \xi_0). \quad (41)$$

In that case, it presents a core [see Fig. 1(b)]. Moreover, for $d > 2$, the asymptotic behavior of the solution for $\xi \rightarrow +\infty$ is the same as for the isothermal self-gravitating gas without a central body [38]. The reason is that an unbounded isothermal self-gravitating gas carries out an infinite mass so the effect of the central body becomes negligible at sufficiently large distances. As a result, the solution behaves as [38]

$$e^{-\psi} \sim \frac{2(d-2)}{\xi^2} \quad \text{for } \xi \rightarrow +\infty. \quad (42)$$

The particular dimensions $d = 1$ and $d = 2$ are treated specifically in a companion paper [90].

C. The fundamental equation of hydrostatic equilibrium

We can obtain the spatial structure of a self-gravitating gas surrounding a central body in a different (but equivalent) manner by starting directly from the condition of hydrostatic equilibrium (for $R_* < r < R$):

$$\nabla P + \rho \nabla \Phi_{\text{tot}} = \mathbf{0}. \quad (43)$$

Dividing Eq. (43) by ρ , taking its divergence, and using the Poisson equation

$$\Delta \Phi_{\text{tot}} = S_d G \rho, \quad (44)$$

we obtain

$$\nabla \cdot \left(\frac{\nabla P}{\rho} \right) = -S_d G \rho, \quad (45)$$

which is the fundamental equation of hydrostatic equilibrium. For the isothermal equation of state (22), it takes the form

$$\frac{k_B T}{m} \Delta \ln \rho = -S_d G \rho. \quad (46)$$

For a spherically symmetric distribution, we get

$$\frac{1}{r^{d-1}} \frac{d}{dr} \left(r^{d-1} \frac{d \ln \rho}{dr} \right) = -S_d \beta G m \rho, \quad (47)$$

with the boundary condition

$$\left(\frac{d \ln \rho}{dr} \right) (R_*) = -\beta m \frac{GM_*}{R_*^{d-1}} \quad (48)$$

obtained from Eqs. (22), (28), and (43). Writing $\rho(r) = \rho_0 e^{-\psi(\xi)}$ with the variables ψ and ξ defined previously, we recover the Emden equation (35) with the boundary condition (36). The two descriptions are of course equivalent since the condition of hydrostatic equilibrium (43) can be obtained by taking the logarithmic derivative of Eq. (23) and using Eq. (22). More generally, it is satisfied by any distribution function that only depends on the individual energy of the particles: $f(\mathbf{r}, \mathbf{v}) = f(\epsilon)$ where $\epsilon = v^2/2 + \Phi(\mathbf{r})$ (see Appendix C).

D. The Milne variables

Let us introduce the analog of the Milne variables

$$u = \frac{d \ln M_{\text{tot}}(r)}{d \ln r}, \quad v = -\frac{d \ln P(r)}{d \ln r}, \quad (49)$$

where $M_{\text{tot}}(r) = M(r) + M_*$ is the total mass enclosed within the sphere of radius r and $P(r) = \rho(r) k_B T / m$ is the local

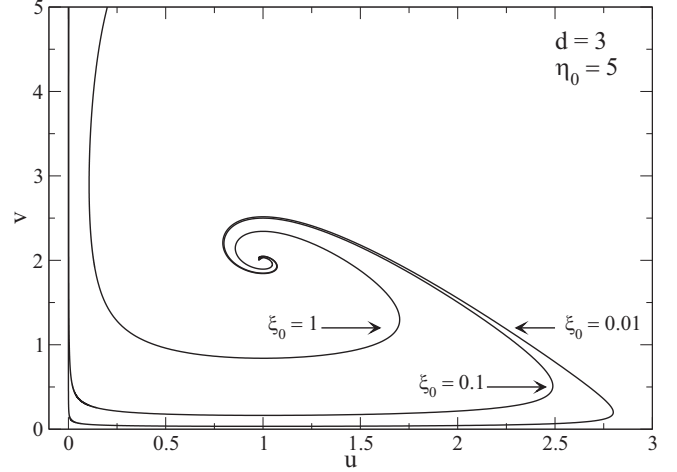


FIG. 2. Solution of the Emden equation with a central body in the (u, v) plane in $d = 3$ dimensions (we have selected $\eta_0 = 5$ for illustration).

pressure. Using the equalities $GM_{\text{tot}}(r) = r^{d-1} d\Phi_{\text{tot}}/dr$ and $dM_{\text{tot}}/dr = S_d r^{d-1} \rho(r)$ (see Appendix D), we easily find that

$$u = \frac{\xi e^{-\psi}}{\psi'}, \quad v = \xi \psi'. \quad (50)$$

Therefore, the Milne variables keep the same form as in the absence of central body [38,45]. They satisfy the first-order differential equation

$$\frac{u dv}{v du} = \frac{2-d+u}{d-u-v}. \quad (51)$$

The (u, v) curves are parameterized by ξ . They start from $(\xi_0^2/\eta_0, \eta_0)$ for $\xi = \xi_0$ and end at $(d-2, 2)$ for $\xi \rightarrow +\infty$ (if $d > 2$). An example of (u, v) curve is shown in Fig. 2.

E. The thermodynamical parameters

For $d > 2$, there is no global entropy maximum at fixed mass and energy in an unbounded domain. The isothermal gas surrounding the central body has the tendency to evaporate, leading to higher and higher values of entropy as the volume that it occupies increases. There are not even extrema of entropy at fixed mass and energy in an unbounded domain because the solutions of the Boltzmann-Poisson equation (24) have infinite mass. As in the case without central body, we shall confine the gas within a box of radius R . The box delimitates the region where the system is isolated from the surrounding so that thermodynamical arguments can be applied. It can mimic the effect of a tidal radius for globular clusters and dark matter halos, or represent the Hill sphere in the context of planet formation. In the context of the chemotaxis of bacterial populations, the box has a physical justification as it represents the domain containing the bacteria.

In a bounded domain, the solutions of the Emden equation (35) are terminated by the box at a normalized radius given by

$$\alpha = (S_d G \beta m \rho_0)^{1/2} R. \quad (52)$$

Using Eqs. (8) and (52), we can rewrite Eq. (37) as

$$\xi_0 = \alpha \zeta, \quad \eta_0 = \frac{\eta \mu}{\zeta^{d-2}}. \quad (53)$$

We shall now relate α to the dimensionless temperature η and to the dimensionless energy Λ .

1. The temperature

According to the Newton law (30) applied at $r = R$, we have

$$\frac{d\Phi_{\text{tot}}}{dr}(R) = \frac{G(M_* + M)}{R^{d-1}}, \quad (54)$$

where M is the total mass of the gas. Introducing the variables defined previously and using $\xi = r\alpha/R$, the foregoing relation can be rewritten as

$$\eta = \frac{\alpha \psi'(\alpha)}{1 + \mu}. \quad (55)$$

This relation can also be obtained by substituting the Boltzmann distribution (33) into the mass constraint (6) and by using the Emden equation (35).

2. The energy

The computation of the energy is a little more intricate. Using the Maxwell-Boltzmann distribution (21), or the isothermal equation of state (22), the kinetic energy

$$E_{\text{kin}} = \int f \frac{v^2}{2} d\mathbf{r} dv = \frac{d}{2} \int P d\mathbf{r} \quad (56)$$

is given by

$$E_{\text{kin}} = \frac{d}{2} N k_B T, \quad (57)$$

just like for a noninteracting (perfect) gas. Therefore, the dimensionless kinetic energy is

$$-\frac{E_{\text{kin}} R^{d-2}}{GM^2} = -\frac{d}{2\eta}. \quad (58)$$

The potential energy $W_{\text{tot}} = W + W_{\text{ext}}$ is given by

$$W_{\text{tot}} = \frac{1}{2} \int \rho \Phi d\mathbf{r} + \int \rho \Phi_{\text{ext}} d\mathbf{r}. \quad (59)$$

Using Eq. (25) it can be rewritten as

$$W_{\text{tot}} = \frac{1}{2} \int \rho \Phi_{\text{tot}} d\mathbf{r} + \frac{1}{2} \int \rho \Phi_{\text{ext}} d\mathbf{r}. \quad (60)$$

We shall compute the potential energy in two different manners, either by using the virial theorem or by directly evaluating the integral (60). The first approach based on the virial theorem is only valid for $d \neq 2$ while the second approach is general.

For $d \neq 2$, it is shown in Appendix B that the virial theorem for a self-gravitating gas in hydrostatic equilibrium surrounding a central body can be written as

$$2E_{\text{kin}} + (d-2)W_{\text{tot}} = dP(R)V - dP(R_*)V_*, \quad (61)$$

where $V = S_d R^d/d$ is the volume of the box enclosing the gas and $V_* = S_d R_*^d/d$ is the volume of the central body. This relation is valid for a general equation of state. For the isothermal

equation of state (22), we obtain

$$2E_{\text{kin}} + (d-2)W_{\text{tot}} = S_d(\rho(R)R^d - \rho_0 R_*^d) \frac{k_B T}{m}, \quad (62)$$

where the first term (kinetic energy) is given by Eq. (57). This equation then determines the potential energy W_{tot} . Introducing the dimensionless variables defined previously, we get

$$-\frac{W_{\text{tot}} R^{d-2}}{GM^2} = \frac{\alpha^2}{(d-2)\eta^2} (\zeta^d - e^{-\psi(\alpha)}) + \frac{d}{d-2} \frac{1}{\eta}. \quad (63)$$

The total energy is $E = E_{\text{kin}} + W_{\text{tot}}$. Adding Eqs. (58) and (63), we find that the total dimensionless energy is given by

$$\Lambda = \frac{4-d}{d-2} \frac{d}{2\eta} + \frac{\alpha^2}{(d-2)\eta^2} (\zeta^d - e^{-\psi(\alpha)}) \quad (d \neq 2). \quad (64)$$

It can be useful to obtain another expression of the energy. Introducing the dimensionless variables defined previously in the expression of the potential energy (60), and using Eq. (B3) for $d \neq 2$, we find that the dimensionless potential energy can be written as

$$-\frac{W_{\text{tot}} R^{d-2}}{GM^2} = -\frac{1}{2\eta^2 \alpha^{d-2}} \int_{\alpha\zeta}^{\alpha} (\psi + \psi_*) e^{-\psi} \xi^{d-1} d\xi + \frac{\mu}{2(d-2)\eta} \int_{\alpha\zeta}^{\alpha} e^{-\psi} \xi d\xi. \quad (65)$$

The quantity $\psi_* \equiv \beta m \Phi_{\text{tot}}(R_*)$ is obtained by evaluating $\psi(\xi) = \beta m \Phi_{\text{tot}}(r) - \psi_*$ at $\xi = \alpha$, using $\Phi_{\text{tot}}(R) = -[1/(d-2)]GM_{\text{tot}}/R^{d-2}$ (see Appendix D) for $d \neq 2$. This yields

$$\psi_* = -\frac{\eta(1+\mu)}{d-2} - \psi(\alpha). \quad (66)$$

Adding Eqs. (58) and (65), we find that the total dimensionless energy is given by

$$\Lambda = -\frac{d}{2\eta} - \frac{1}{2\eta^2 \alpha^{d-2}} \int_{\alpha\zeta}^{\alpha} (\psi + \psi_*) e^{-\psi} \xi^{d-1} d\xi + \frac{\mu}{2(d-2)\eta} \int_{\alpha\zeta}^{\alpha} e^{-\psi} \xi d\xi \quad (d \neq 2). \quad (67)$$

This expression is equivalent to Eq. (64), but it is more complicated since it involves new integrals. However, the present method can be generalized in $d = 2$ dimensions.

Using Eq. (B4) for $d = 2$, the dimensionless potential energy (60) can be written as

$$-\frac{W_{\text{tot}}}{GM^2} = -\frac{1}{2\eta^2} \int_{\alpha\zeta}^{\alpha} (\psi + \psi_*) e^{-\psi} \xi d\xi - \frac{\mu}{2\eta} \int_{\alpha\zeta}^{\alpha} e^{-\psi} \ln(\xi/\alpha) \xi d\xi. \quad (68)$$

The quantity $\psi_* \equiv \beta m \Phi_{\text{tot}}(R_*)$ is obtained by evaluating $\psi(\xi) = \beta m \Phi_{\text{tot}}(r) - \psi_*$ at $\xi = \alpha$, using $\Phi_{\text{tot}}(R) = 0$ (see Appendix D). This yields

$$\psi_* = -\psi(\alpha). \quad (69)$$

Adding Eqs. (58) and (68), we find that the total dimensionless energy is given by

$$\Lambda = -\frac{1}{\eta} - \frac{1}{2\eta^2} \int_{\alpha\zeta}^{\alpha} (\psi + \psi_*) e^{-\psi} \xi d\xi + \frac{1}{2} \mu \ln \alpha - \frac{\mu}{2\eta} \int_{\alpha\zeta}^{\alpha} e^{-\psi} \xi \ln \xi d\xi \quad (d=2). \quad (70)$$

The virial theorem in $d=2$ is discussed in Ref. [90].

F. Entropy and free energy

The entropy and the free energy (or Massieu function) of the equilibrium state can be calculated as follows. From Eqs. (12) and (21) we get

$$S_B/k_B = \alpha_0 M + \left(\frac{d}{2} + 1\right) N + 2\beta W + \beta W_{\text{ext}}, \quad (71)$$

where we have used Eqs. (56) and (57). Applying Eq. (23) at $r=R$ and using Eqs. (7), (33), (52) and $\Phi(R) + \Phi_{\text{ext}}(R) = -G(M + M_*)/[(d-2)R^{d-2}]$ for $d \neq 2$ or $\Phi(R) + \Phi_{\text{ext}}(R) = 0$ for $d=2$ [see Eqs. (B3), (B4), (D9), and (D10)], we find that

$$\alpha_0 m = -2 \ln \alpha - \left(\frac{d}{2} - 1\right) \ln \eta + \psi(\alpha) + \frac{\eta}{d-2} (1 + \mu) + \ln[(2\pi)^{d/2} S_d G^{d/2} M^{(d-2)/2} m R^{(4-d)d/2}] - 1. \quad (72)$$

We also have

$$E = \frac{d}{2} N k_B T + W_{\text{tot}}, \quad (73)$$

with $W_{\text{tot}} = W + W_{\text{ext}}$. From Eqs. (7) and (73) we obtain

$$2\beta W + \beta W_{\text{ext}} = -2N\Lambda\eta - dN - \beta W_{\text{ext}}. \quad (74)$$

Substituting Eqs. (72) and (74) into Eq. (71) we find that

$$S_B/Nk_B = -\left(\frac{d}{2} - 1\right) \ln \eta - 2 \ln \alpha + \psi(\alpha) + \frac{1}{d-2} (1 + \mu) \eta - 2\Lambda\eta - \frac{d}{2} - \frac{\beta W_{\text{ext}}}{N} + \ln[(2\pi)^{d/2} S_d G^{d/2} M^{(d-2)/2} m R^{(4-d)d/2}]. \quad (75)$$

The term $\beta W_{\text{ext}}/N$ can be obtained from Eqs. (8), (33), (34), (53), (B3), and (B4), yielding

$$\frac{\beta W_{\text{ext}}}{N} = -\frac{1}{d-2} \mu \int_{\alpha\zeta}^{\alpha} e^{-\psi} \xi d\xi \quad (d \neq 2), \quad (76)$$

$$\frac{\beta W_{\text{ext}}}{N} = \mu \int_{\alpha\zeta}^{\alpha} e^{-\psi} \ln(\xi/\alpha) \xi d\xi \quad (d=2). \quad (77)$$

The Massieu function (14) is then given by

$$\frac{J_B}{N} = \frac{S_B}{Nk_B} + \Lambda\eta. \quad (78)$$

G. The structure of the gas profile close to the central body

In this section, we determine the profile of the gas in the vicinity of the central body. The density profile of the isothermal gas is given by the Boltzmann distribution

$$\rho(r) = A e^{-\beta m \Phi_{\text{tot}}(r)}, \quad (79)$$

where $\Phi_{\text{tot}} = \Phi + \Phi_{\text{ext}}$ is the total gravitational potential. For $r \rightarrow R_*$, the gravitational potential is dominated by the contribution of the central body $\Phi_{\text{ext}}(r)$ so that¹²

$$\Phi_{\text{tot}}(r) \simeq -\frac{1}{d-2} \frac{GM_*}{r^{d-2}} \quad (d \neq 2), \quad (80)$$

$$\Phi_{\text{tot}}(r) \simeq GM_* \ln(r/R) \quad (d=2). \quad (81)$$

For $d=1$, we find that the density profile close to the central body increases exponentially rapidly as

$$\rho(x) = \rho_0 e^{-(x-R_*)/\epsilon} \quad (82)$$

on a typical length scale

$$\epsilon = \frac{1}{\beta G m M_*}. \quad (83)$$

This corresponds to a ‘‘cusp’’ since the first derivative $\rho'(R_*) = -\rho_0/\epsilon$ of the density profile is nonzero at $x=R_*$. This solution remains valid if the central body is a Dirac mass ($R_* = 0$) in which case $\rho = \rho_0 e^{-x/\epsilon}$ for $x \rightarrow 0$ [90].

For $d=2$, we find that the density profile close to the central body increases like a power law:

$$\rho(r) = \rho_0 \left(\frac{R_*}{r}\right)^{\beta G M_* m}. \quad (84)$$

Again, we have a cusp since $\rho'(R_*) = -\beta G M_* m \rho_0 / R_* \neq 0$. This power-law behavior remains valid if the central body is a Dirac mass ($R_* = 0$) in which case $\rho(r) = A r^{-\beta G M_* m}$. The density diverges at $r=0$ and the profile is normalizable provided that $\beta G M_* m < 2$ [90].

For $d=3$, we find that the density profile close to the central body is

$$\rho(r) = \rho_0 e^{\beta G M_* m (\frac{1}{r} - \frac{1}{R_*})}. \quad (85)$$

We note that the density profile is not normalizable in the case where the central body is a Dirac mass ($R_* = 0$). For $r \rightarrow R_*$, we find that the density profile increases exponentially rapidly as

$$\rho(r) = \rho_0 e^{-(r-R_*)/\epsilon} \quad (86)$$

on a typical length scale

$$\epsilon = \frac{R_*^2}{\beta G M_* m}. \quad (87)$$

Therefore, at the contact with the central body, there is a density *spike* (or cusp) of the gas on a typical length ϵ since $\rho'(R_*) = -\rho_0/\epsilon \neq 0$. Then, taking $r \rightarrow +\infty$ in Eq. (85), we find that the spike is followed by a *plateau* where the density is nearly constant:

$$\rho = \rho_0 e^{-\frac{\beta G M_* m}{R_*}}. \quad (88)$$

This plateau extends on a typical length L such that the mass of gas contained in this region becomes comparable to the mass of the central body. This corresponds to the condition

$$\rho_0 e^{-\frac{\beta G M_* m}{R_*}} \frac{4}{3} \pi (L^3 - R_*^3) = M_*. \quad (89)$$

¹²A better approximation may consist in replacing M_* by $M_{\text{tot}}(r)$ in the following formulas.

If $R_* \ll L$, then we get the estimate

$$L \simeq \left(\frac{3M_*}{4\pi\rho_0} \right)^{1/3} e^{\frac{\beta GM_* m}{3R_*}}. \quad (90)$$

For $r > L$, the self-gravity of the gas must be taken into account and, at large distances, the density decreases with a typical r^{-2} behavior corresponding to the standard self-gravitating isothermal sphere [45]. This “cusp + plateau + halo” structure (or simply “cusp-halo” structure) is clearly visible in Fig. 1. These results are similar to those found in the case of self-gravitating fermions [60,95] where the role of the central body is played by the completely degenerate fermion ball (quantum core).

From these considerations, we can distinguish four types of configurations which are reminiscent of the morphology of certain objects in planetology:

(i) If the mass of the central body is small (or if there is no central body) and if the gas is not too dense, then we have a non-self-gravitating homogeneous gas that could represent a diffuse nebula.

(ii) If the mass of the central body is large and if the gas is not too dense, then we have a non-self-gravitating gas experiencing only the gravitational potential of the central body (solid planetary core). The density of the gas increases rapidly at the contact of the solid core and forms a spike. A massive solid core surrounded by a tiny atmosphere corresponds to the structure of telluric planets like the Earth.

(iii) If the mass of the central body is small (or if there is no central body) and if the gas is sufficiently dense, then we have a standard isothermal self-gravitating gas (isothermal sphere) with a finite central density. It could represent a protoplanet.

(iv) If the mass of the central body is large and if the gas is sufficiently dense, then we have a self-gravitating gas experiencing the gravitational potential of the central body (solid planetary core). The density of the gas increases rapidly at the contact of the solid core and forms a spike. This thin layer is then followed by an envelope held by its self-gravity. This corresponds to the structure of giant planets like Jupiter and Saturn.

Cases (i) and (iii) correspond to the “gaseous phase” where the influence of the central object is weak. Cases (ii) and (iv) correspond to the “condensed phase” where the influence of the central object is strong. In that case, the density of the gas is enhanced close to the solid core and forms a spike. The gaseous phase and the condensed phase can themselves be divided in two categories depending on whether the envelope is self-gravitating or not.

The case of globular clusters and dark matter halos, which are self-gravitating, corresponds to points (iii) and (iv) depending whether they contain a central black hole or not.

H. The numerical procedure

To plot the series of equilibria $\eta(\Lambda)$ for fixed external parameters ζ and μ , we proceed as follows: (i) We fix ξ_0 and make a guess η_0^{guess} for η_0 ; (ii) we solve the Emden equation (35) with the boundary condition from Eq. (36) until $\alpha = \xi_0/\zeta$. This gives η and Λ according to the formulas of Sec. II E and $\eta_0 = \eta\mu/\zeta^{d-2}$. We iterate this procedure until the values of η_0^{guess} and η_0 coincide; (iii) in that case, the

chosen value of ξ_0 determines α , η and Λ . By varying ξ_0 , we can obtain the whole series of equilibria $\eta(\Lambda)$ for given values of ζ and μ .

III. CALORIC CURVES AND PHASE TRANSITIONS IN THE PRESENCE OF A CENTRAL BODY IN $d = 3$ DIMENSIONS

In this section, we describe phase transitions which take place in a self-gravitating system with a central body in $d = 3$ dimensions. We fix the typical density of the central body, $\rho_* = M_*/R_*^3$, and plot the series of equilibria $\beta(E)$ for different values of the radius R_* of the central body. We could also fix the mass M_* of the central body instead of its average density, but we think that fixing the average density is more relevant if we want to apply our results, for example, to the problem of planet formation.¹³ Furthermore, the classical isothermal gas without central body [9,15] is recovered for $R_* \rightarrow 0$ with fixed ρ_* while the limit $R_* \rightarrow 0$ with fixed M_* corresponds to a central Dirac mass. This corresponds to a very different situation.

The dimensionless density of the central body is

$$\kappa \equiv \frac{M_* R_*^3}{M R_*^3} = \frac{\mu}{\zeta^3}. \quad (91)$$

We shall work with the dimensionless variables defined previously. However, it may be useful in the discussion to take $M = R = G = m = 1$ (we can always introduce appropriate scales to be in this situation). In that case, $\zeta = R_*$ represents the radius of the central body, $\kappa = \rho_*$ the density of the central body, $\eta = \beta$ the inverse temperature of the gas and $\Lambda = -E$ the energy of the gas (with the opposite sign). In the discussion, we shall use the physical variables R_* , ρ_* , β , and E , and in the figures, we shall use the dimensionless variables ζ , κ , η , and Λ .

In Figs. 3 and 4, we plot the curve $\beta(E)$ for a fixed central body density ρ_* and for different values of the central body radius R_* . This curve contains all the extrema of entropy (respectively, free energy) at fixed mass and energy (respectively, temperature). For that reason, it is called the *series of equilibria*. The series of equilibria is parameterized by the density contrast $\mathcal{R} = \rho_0/\rho(R) = e^{\psi(\alpha)}$ between the central body and the box. The stable part of this curve in each ensemble defines the *caloric curve*. The series of equilibria (extremal states) is the same in the canonical and microcanonical ensembles while the caloric curve (stable states) can be different in case of ensemble inequivalence. For $R_* \rightarrow 0$, we recover the classical spiral of a self-gravitating isothermal gas without central body [1–5]. For finite R_* , the spiral unwinds and different shapes are possible depending on the value of R_* . For $R_* < R_*^{\text{MCP}}$, the curve has a Z-shape structure leading to zeroth and first-order microcanonical and canonical phase transitions. At the microcanonical critical point $R_* = R_*^{\text{MCP}}$, the microcanonical phase transitions disappear. For $R_*^{\text{MCP}} < R_* < R_*^{\text{CCP}}$, the

¹³Rocky cores have a given typical density $\rho_* = M_*/R_*^3$ determined by their composition. By contrast, a central black hole has a constant mass to radius ratio $M_*/R_* = c^2/2G$ determined by the Schwarzschild relation.

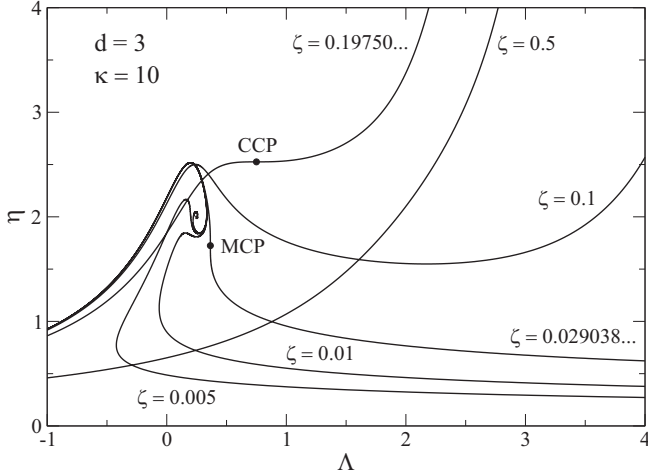


FIG. 3. Series of equilibria at fixed central body density κ (we have taken $\kappa = 10$ for illustration) for several values of the central body radius ζ . As ζ increases, the series of equilibria unwinds. There exists a microcanonical critical point (MCP) and a canonical critical point (CCP) above which the microcanonical and the canonical phase transitions respectively disappear.

curve has an N -shape structure leading to zeroth and first-order canonical phase transitions. At the canonical critical point $R_* = R_*^{\text{CCP}}$, the canonical phase transitions disappear. Finally, for $R_* > R_*^{\text{CCP}}$, the curve is monotonic so that there is no phase transition anymore. In that case, the statistical ensembles are equivalent.

We see that the description of phase transitions in a self-gravitating classical gas with a central body is very similar to that already given for self-gravitating fermions [5]. The central body provides a small scale regularization of the gravitational force that prevents complete collapse and the formation of singularities. In that sense, it has an effect similar to the Pauli exclusion principle in quantum mechanics or to the core radius of the particles in a hard spheres gas. Since the phenomenology is the same in all these situations,

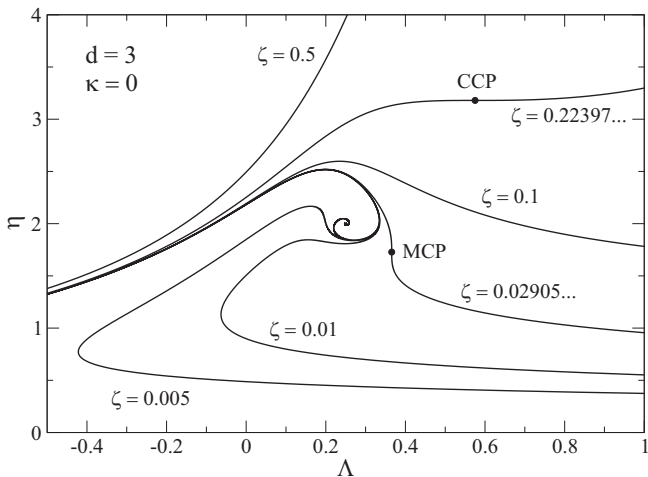


FIG. 4. Same as Fig. 3 for $\kappa = 0$ and $\zeta \neq 0$ (hole). This corresponds to a system of self-gravitating particles contained in a volume delimited by two shells at radii $r = R_*$ and $r = R$.

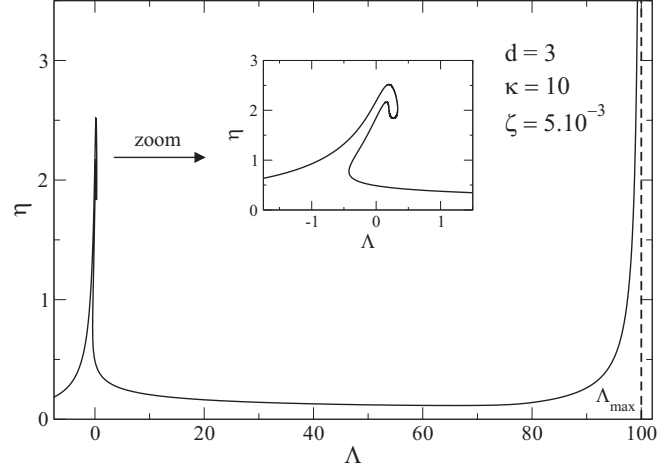


FIG. 5. Series of equilibria for $\kappa = 10$ and $\zeta = 5 \times 10^{-3} < \zeta_{\text{MCP}}$. It has a characteristic Z-shape structure (“dinosaur’s neck” [5]). There exists an equilibrium state for all accessible values of the energy $\Lambda \leq \Lambda_{\text{max}}(\zeta, \kappa)$ in the microcanonical ensemble, and for all values of temperature $\eta \geq 0$ in the canonical ensemble. However, interesting phase transitions, described in the text, appear for energies around Λ_c and temperatures around η_c (see the following figures).

we shall be relatively brief and refer to the review [5] for more details about phase transitions in self-gravitating systems. We note, however, that in the present case, the structure of the series equilibria $\beta(E)$ depends on two parameters ρ_* and R_* characterizing the central body while in the case of self-gravitating fermions there is only one parameter $\mu = (gm^4/h^3)\sqrt{512\pi^4 G^3 MR^3}$ related to the inverse of the Planck constant ($\mu \sim 1/\hbar^3$) or to the ratio $\mu \sim (R/R_*)^{3/2}$ between the system size R and the size R_* of a fermion ball (a self-gravitating Fermi gas at $T = 0$) with mass M . Furthermore, in the present case, the central body is an external object distinct from the gas while the fermion ball (or the solid core) is created by the system itself. What plays the role of the condensed object in the present context is the cusp at the contact with the central body (there is also a cusp in the case of self-gravitating fermions [95]).

A. The case of a small central body $R_* < R_*^{\text{MCP}}$ in the microcanonical ensemble: Z-shape structure

We first consider the case of a small central body $R_* < R_*^{\text{MCP}}$ so that the series of equilibria has a Z-shape structure resembling a “dinosaur’s neck” [5] (see Figs. 5 and 6).

In this section, we consider the case of an isolated system so that the control parameter is the energy and the relevant statistical ensemble is the microcanonical ensemble. As explained previously, the series of equilibria contains all the extrema of entropy at fixed mass and energy. The thermodynamically stable states in the microcanonical ensemble correspond to entropy *maxima* at fixed mass and energy (minima or saddle points of entropy must be discarded). They can be determined by applying the turning point method of Poincaré (see, e.g., Refs. [4,5]). At very high energies, self-gravity is negligible with respect to thermal motion (velocity dispersion) and the system is equivalent to a noninteracting

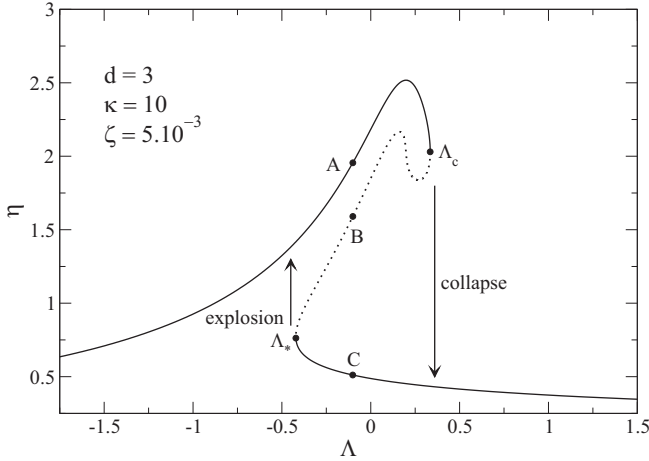


FIG. 6. Physical caloric curve in the microcanonical ensemble (solid lines) containing stable (global entropy maxima) and metastable (local entropy maxima) equilibrium states. Unstable saddle points of entropy are represented by dotted lines.

gas in a box. We know from ordinary thermodynamics that this gas is stable (entropy maximum). Therefore, using the Poincaré criterion, we conclude that the upper branch of the series of equilibria is stable (entropy maxima at fixed mass and energy) until the first turning point of energy E_c where the tangent is vertical. For sufficiently small values of R_* , this is close to the Antonov energy -0.335 [1,9]. At that point, the curve $\beta(-E)$ rotates clockwise so that a mode of stability is lost.¹⁴ Therefore, the configurations in the intermediate branch are unstable saddle points of entropy at fixed mass and energy. However, at the second turning point of energy E_* , the curve $\beta(-E)$ rotates anti-clockwise so that the mode of stability is regained. Therefore, the lower branch is stable (entropy maxima at fixed mass and energy). The energy E_* depends on R_* and tends to $E_*(R_*) \rightarrow +\infty$ when $R_* \rightarrow 0$.

Typical density profiles of the series of equilibria are shown in Fig. 7. The states (A) on the upper branch have an almost uniform density with a small density contrast $\mathcal{R} = \rho(R_*)/\rho(R)$. They form the *gaseous phase*. At large distances, their density profile decreases approximately like r^{-2} . The states (C) on the lower curve are highly inhomogeneous. They present a high-density cusp at the contact with the central body surrounded by a dilute atmosphere. Therefore, the density contrast $\mathcal{R} = \rho(R_*)/\rho(R)$ is large. They form the *condensed phase*. They have a “cusp-halo” structure which is the counterpart of the “core-halo” structure of self-gravitating fermions (in that case the core is a degenerate quantum body). The cusp contains a lot of potential energy. By forming the cusp, some energy is released in the form of kinetic energy in

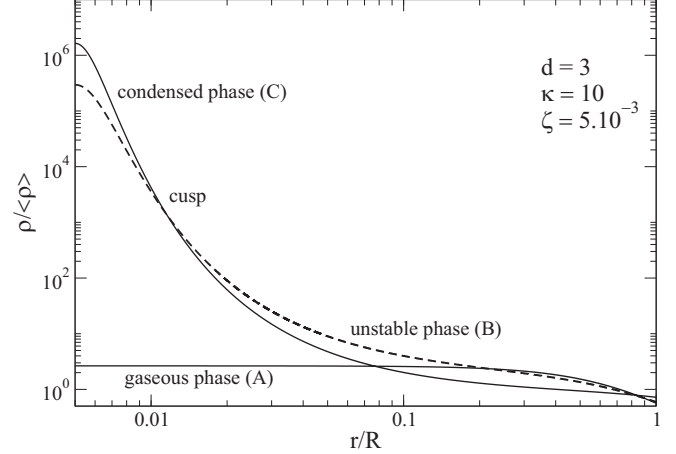


FIG. 7. Typical normalized density profiles $\rho/\langle\rho\rangle$ with $\langle\rho\rangle = 3M/4\pi R^3$ corresponding to gaseous (points A), condensed (points C) and unstable (points B) states. The condensed and unstable states have a cusp-halo structure.

the halo which is very hot and almost uniform. This explains the plateau following the cusp (see Sec. II G). Finally, the states (B) on the intermediate (unstable) branch are similar to the gaseous states (the density profile decreases approximately like r^{-2} at large distances) except that they form an embryonic cusp at the contact with the core. This is the equivalent of a “germ” in the language of phase transitions (see below).

In Fig. 8, we have plotted the inverse temperature β minus the energy $-E$ as a function of the central density $\rho_0 = \rho(R_*)$ (more precisely the value of the density of the gas at the contact with the central body). The central density parameterizes the series of equilibria. We clearly see the appearance of oscillations giving rise to the spiral on the series of equilibria. They lead to microcanonical instability at the first turning point of energy and to canonical instability at the first turning point of temperature (stability is regained at the last turning points).

In principle, to obtain the caloric curve, we must determine which states are local entropy maxima and which states are global entropy maxima. This can be done by performing a vertical Maxwell construction or by plotting the entropy of the two phases as a function of the energy and determining the transition energy E_t at which they become equal [5]. The *strict caloric curve* in the microcanonical ensemble is obtained by keeping only fully stable states (global entropy maxima), as in Fig. 9. From this curve, we would expect a first-order microcanonical phase transition to occur at $E = E_t$, connecting the gaseous phase to the condensed phase. It would be accompanied by a discontinuity of temperature and specific heat. However, for self-gravitating systems, the metastable states are long-lived because the probability of a fluctuation able to trigger the phase transition is extremely weak. Indeed, to trigger a phase transition between a gaseous state and a condensed state, the system has to overcome the entropic barrier played by the solution of the intermediate branch (points B) with a “germ.” Now, the height of the entropic barrier scales like N so that the probability of transition scales like e^{-N} . Therefore, metastable states (local entropy maxima) are very robust

¹⁴We note that the region of negative specific heat just before the first turning point of energy is stable in the microcanonical ensemble. The system becomes unstable in the microcanonical ensemble after the first turning point of energy when the specific heat becomes positive. The regions of negative specific heat and the situations of ensemble inequivalence will be discussed in more detail in the following sections.

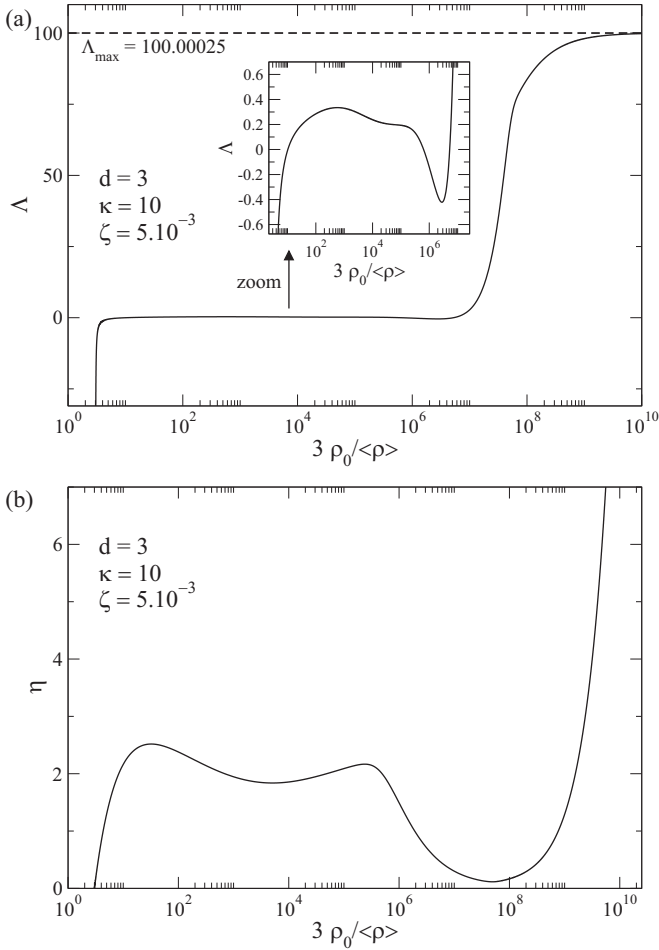


FIG. 8. Evolution of the energy Λ and the inverse temperature η as a function of the normalized central density $\rho_0/\langle\rho\rangle$.

[26] because their lifetime scales like the exponential of the number of particles, $t_{\text{life}} \sim e^N$, and it becomes infinite at the thermodynamic limit $N \rightarrow +\infty$. In practice, the first-order phase transition at E_t does *not* take place and, for sufficiently large N , the system remains “frozen” in the metastable phase. Therefore, the *physical caloric curve* in the microcanonical ensemble must take into account the metastable states (local entropy maxima) which are as much relevant as the fully stable equilibrium states (global entropy maxima). This physical caloric curve is multi-valued and corresponds to the solid lines in Fig. 6. It is obtained from the series of equilibria by discarding the unstable saddle points (dashed line).

Reducing progressively the energy from high values (for unbounded systems, the mechanism by which energy decreases may be due physically to a slow evaporation), the system remains in the gaseous phase (points A) until the critical value E_c at which the gaseous phase ceases to exist. At that point, called a spinodal point, the system undergoes a gravothermal catastrophe [15]. However, in the present case, complete collapse is prevented by the central body and the systems ends up in the condensed phase (points C). Since the gravitational collapse is accompanied by a discontinuous jump of entropy this phase transition is of zeroth order. The resulting equilibrium state has a “cusp-halo” structure. The

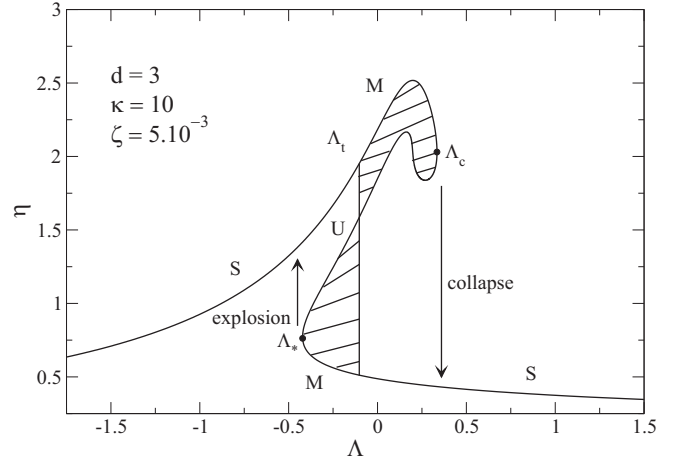


FIG. 9. Caloric curve in the microcanonical ensemble. We have indicated the fully stable states (global entropy maxima S), the metastable states (local entropy maxima M) and the unstable states (saddle points U). The strict caloric curve is composed by the fully stable states and exhibits a first-order phase transition at Λ_t . In practice, this phase transition does not take place because the metastable states have a very long lifetime. The physical caloric curve is composed of the fully stable and metastable states (see Fig. 6). The ends of the metastable branches are called spinodal points. At these points, the system exhibits zeroth order phase transitions associated with a collapse and an explosion.

cusp contains a small fraction of the mass and this fraction decreases as $R_* \rightarrow 0$ (in the absence of a central body, the gravothermal catastrophe leads to a *binary star* with a small mass but a large binding energy [5]). The rest of the mass is diluted in a hot and massive envelope held by the box. In an open system (i.e., if the box is removed) the halo would be dispersed at infinity so that only the cusp (thin atmosphere) would remain. If we now increase the energy of the gas (for unbounded systems, the mechanism to supply energy could be due to an accretion), then the system remains in the condensed phase until the critical value E_* at which the condensed phase ceases to exist. At that second spinodal point, the system undergoes an explosion, reverse to the collapse, and returns to the gaseous phase. Since the collapse and the explosion occur at different values of the energy (due to the presence of metastable states), we can generate an hysteretic cycle in the microcanonical ensemble by varying the energy between E_c and E_* . This hysteretic cycle has been followed numerically by Ispolatov and Karttunen [96] for particles interacting via a softened gravitational potential (the softening regularizes the singularity of the gravitational potential and plays a role similar to that of the central body in our case).

B. The case of a moderate central body $R_*^{\text{MCP}} < R_* < R_*^{\text{CCP}}$ in the microcanonical ensemble: N -shape structure

We now consider the case of a central body of intermediate core radius, $R_*^{\text{MCP}} < R_* < R_*^{\text{CCP}}$, so that the series of equilibria has an N -shape structure (see Fig. 10).

We first describe the structure of the caloric curve in the microcanonical ensemble. In that case, the control parameter is the energy E . For a moderate value of the core radius,

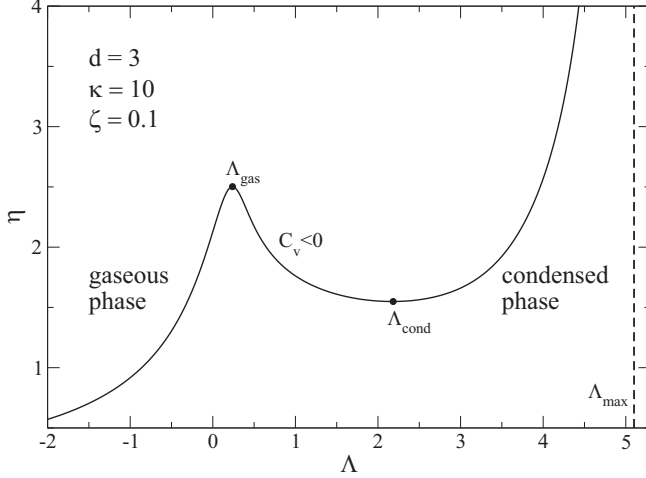


FIG. 10. Caloric curve in the microcanonical ensemble for $\kappa = 10$ and $\zeta_{\text{MCP}} < \zeta = 0.1 < \zeta_{\text{CCP}}$. It has a characteristic N -shape structure. All the solutions are global entropy maxima at fixed mass and energy (fully stable). The solutions between Λ_{gas} and Λ_{cond} have negative specific heats. There is no phase transition in the microcanonical ensemble, only a concentration of the gas near the central body as energy is progressively decreased.

the trace of the classical spiral has almost disappeared and the $\beta(E)$ curve is univalued. Since the solutions are entropy maxima for $E \rightarrow +\infty$, and since there is no turning point of energy (no vertical tangent) in the series of equilibria, we conclude from the Poincaré criterion that all the states are stable and correspond to global entropy maxima at fixed mass and energy. Therefore, for sufficiently large values of the core radius, there is no phase transition in the microcanonical ensemble. The gravothermal catastrophe at E_c is suppressed. However, there is a sort of condensation as the energy is progressively decreased. At high energies, the density profiles are almost homogeneous and they are held by the box. In that case, the specific heat is positive. At smaller energies, the density contrast increases and the system has a “cusp-halo” structure. Between E_{gas} and E_{cond} , the influence of the central body and of the box are weak and these states have negative specific heats. Finally, at low energies, the cusp becomes more and more massive and thin until the minimum energy E_{min} at which all the mass is in contact with the central body (see Appendix F). In that case, the specific heat is positive again.

C. The case of a moderate central body $R_*^{\text{MCP}} < R_* < R_*^{\text{CCP}}$ in the canonical ensemble: N -shape structure

We now describe the structure of the caloric curve in the canonical ensemble for the same values of the parameters as in the previous section. In that case, the control parameter is the temperature T and the reader may find useful to rotate Fig. 10 by 90° to have the control parameter $\eta \sim 1/T$ in abscissa. The series of equilibria $E(T)$ is multi-valued and this gives rise to canonical phase transitions (see Fig. 11). In fact, we are in a situation parallel to the one described in Sec. III A in the microcanonical ensemble, provided that we interchange the role of E and T . The series of equilibria contains all the extrema of free energy at fixed mass. The thermodynamically

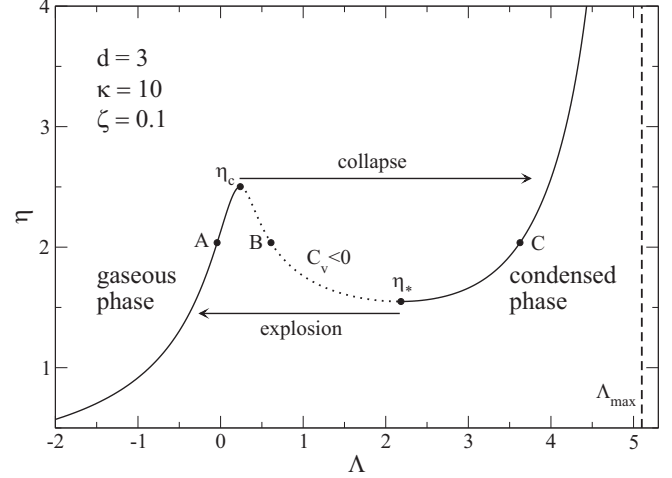


FIG. 11. Physical caloric curve in the canonical ensemble (solid lines) containing stable (global free-energy minima) as well as metastable (local free-energy minima) equilibrium states. Unstable saddle points of free energy at fixed mass are represented by dotted lines and they lie in the region of negative specific heats.

stable states in the canonical ensemble correspond to free-energy *minima* at fixed mass (maxima or saddle points of free energy must be discarded). They can be determined by applying the turning point method of Poincaré. At very high temperatures, self-gravity is negligible with respect to thermal motion and the system is equivalent to a noninteracting gas in a box. We know from ordinary thermodynamics that this gas is stable in every ensemble. Therefore, using the Poincaré criterion, we conclude that the left branch is stable (free-energy minima at fixed mass) until the first turning point of temperature T_c where the tangent is horizontal. For sufficiently small values of R_* , this is close to the Emden inverse temperature 2.52 [34,35]. At that point, the curve $-E(\beta)$ rotates clockwise so that a mode of stability is lost. Therefore, the configurations in the intermediate branch are unstable saddle points of free energy. They lie in the region of negative specific heats which is forbidden (unstable) in the canonical ensemble.¹⁵ However, at the second turning point of temperature T_* , the curve $-E(\beta)$ rotates anti-clockwise so that the mode of stability is regained. Therefore, the right branch is stable (free-energy minima at fixed mass). The temperature T_* depends on R_* and tends to $T_*(R_*) \rightarrow +\infty$ when $R_* \rightarrow 0$.

Typical density profiles of the series of equilibria are shown in Fig. 12. The states (A) on the left branch have almost uniform density profiles and they form the *gaseous phase*. The states (C) on the right branch are highly inhomogeneous with a cusp-halo structure. They form the *condensed phase*. Finally, the states (B) on the intermediate (unstable) branch are similar to the gaseous states except that they contain an embryonic cusp at the contact with the central body. This is the equivalent of a “germ” in the language of phase transitions.

¹⁵Negative specific heat is a sufficient (but not necessary) condition of thermodynamical instability in the canonical ensemble [94].

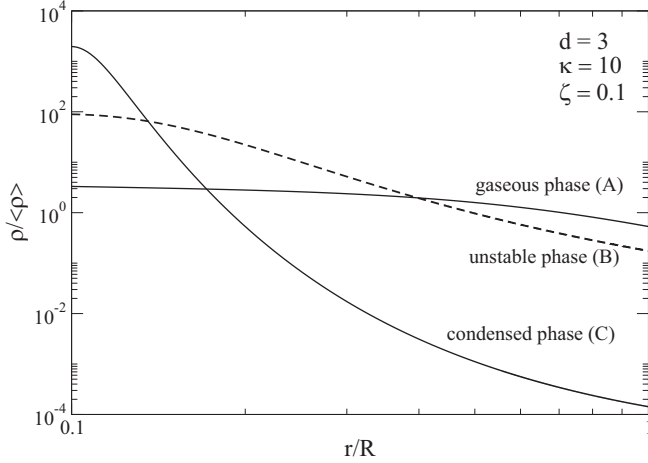


FIG. 12. Typical normalized density profiles $\rho/\langle\rho\rangle$ corresponding to gaseous (points A), condensed (points C) and unstable (points B) states.

In Fig. 13, we have plotted the inverse temperature β and minus the energy $-E$ as a function of the central density $\rho_0 = \rho(R_*)$ (more precisely the value of the density of the gas at the contact with the central body). The central density

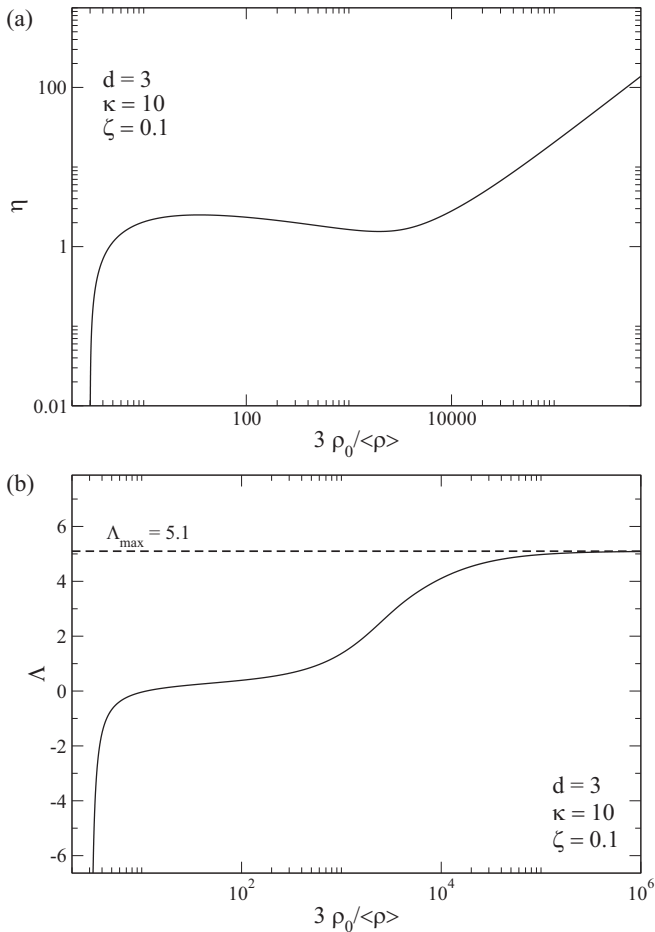


FIG. 13. Evolution of the dimensionless energy Λ and inverse temperature η as a function of the normalized central density $\rho_0/\langle\rho\rangle$.

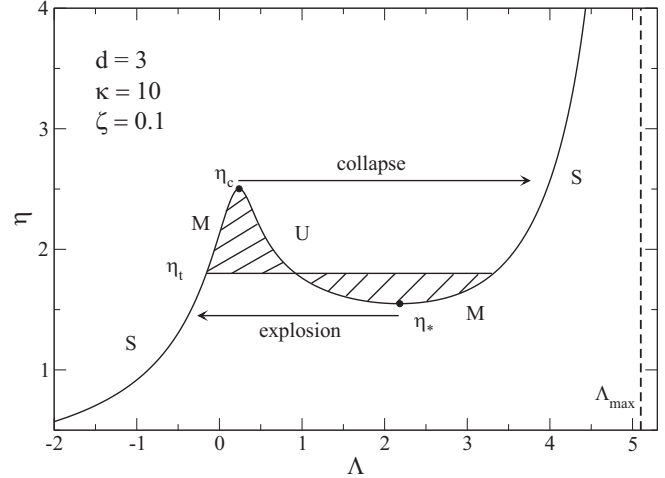


FIG. 14. Caloric curve in the canonical ensemble. We have indicated the fully stable states (global free-energy minima S), the metastable states (local free-energy minima M) and the unstable states (saddle points U). The strict caloric curve is composed by the fully stable states and exhibits a first-order phase transition at η_t which replaces the region of negative specific heats allowed in the microcanonical ensemble (see Fig. 10). In practice, this phase transition does not take place because the metastable states have a very long lifetime. The physical caloric curve is composed of the fully stable and metastable states (see Fig. 11). The ends of the metastable branches are called spinodal points. At these points, the system exhibits zeroth order phase transitions associated with a collapse and an explosion.

parameterizes the series of equilibria. We clearly see the oscillations of $T(\rho_0)$ giving rise to canonical instability at the first turning point of temperature (stability is regained at the last turning point of temperature). On the other hand, the absence of oscillations of $E(\rho_0)$ is associated to full stability in the microcanonical ensemble (see Sec. III C).

In principle, to obtain the caloric curve, we must determine which states are local free-energy minima and which states are global free-energy minima. This can be done by performing a horizontal Maxwell construction or by plotting the free energy of the two phases as a function of the temperature and determining the transition temperature T_t at which they become equal. The *strict caloric curve* in the canonical ensemble is obtained by keeping only fully stable states (global free-energy minima) as in Fig. 14. From this curve, we would expect a first-order canonical phase transition to occur at $T = T_t$, connecting the gaseous phase to the condensed phase. It would be accompanied by a discontinuity of energy and specific heat. Therefore, the region of negative specific heats in the microcanonical ensemble (see Fig. 10) would be replaced by a phase transition (plateau) in the canonical ensemble (see Fig. 14). However, for self-gravitating systems, the metastable states are long-lived because the probability of a fluctuation able to trigger the phase transition is extremely weak. Indeed, to trigger a phase transition between a gaseous state and a condensed state, the system has to overcome the barrier of free energy played by the solutions of the intermediate branch (points B) with a “germ.” Now, the height of the barrier of free energy scales like N so that the

probability of transition scales like e^{-N} . Therefore, metastable equilibrium states (local free-energy minima) are very robust [26] because their lifetime scales like the exponential of the number of particles, $t_{\text{life}} \sim e^N$, and it becomes infinite at the thermodynamic limit $N \rightarrow +\infty$. In practice, the first-order phase transition at T_i does *not* take place and, for sufficiently large N , the system remains “frozen” in the metastable phase. Therefore, the *physical caloric curve* in the canonical ensemble must take into account the metastable states (local free-energy minima) which are as much relevant as the fully stable equilibrium states (global free-energy minima). This physical caloric curve is multi-valued and corresponds to the solid lines in Fig. 11. It is obtained from the series of equilibria by discarding the unstable saddle points (dashed line).

Reducing progressively the temperature from high values, the system remains in the gaseous phase (points A) until the critical value T_c at which the gaseous phase ceases to exist. At that point, called a spinodal point, the system undergoes an isothermal collapse [35]. However, in the present case, complete collapse is prevented by the central body and the system ends up in the condensed phase (points C). Since the gravitational collapse is accompanied by a discontinuous jump of free energy, this phase transition is of zeroth order. The resulting equilibrium state has a “cusp-halo” structure. The cusp contains a large fraction of the mass and this fraction increases as $R_* \rightarrow 0$ (in the absence of a central body, the isothermal collapse leads to a *Dirac peak* containing all the mass [5]). The rest of the mass is diluted in a light envelope held by the box. In an open system (i.e., if the box is removed) the halo would be dispersed to infinity so that only the cusp (thin atmosphere) would remain. If we now increase the temperature of the gas, then the system remains in the condensed phase until the critical value T_* at which the condensed phase ceases to exist. At that second spinodal point, the system undergoes an explosion, reverse to the collapse, and returns to the gaseous phase. Since the collapse and the explosion occur at different values of the temperature (due to the presence of metastable states), one can generate an hysteretic cycle in the canonical ensemble by varying the temperature between T_c and T_* . This hysteretic cycle has been followed numerically by Chavanis *et al.* [74] for a self-gravitating Fermi gas (as we have already indicated, the Pauli exclusion principle plays a role similar to that of the central body in our case).

**D. The case of a large central body $R_* > R_*^{\text{CCP}}$:
Monotonicity and equivalence of statistical ensembles**

We now consider the case of a large central body $R_* > R_*^{\text{CCP}}$ so that the series of equilibria is monotonic (see Fig. 15). In that case, the system does not present any phase transition and the ensembles are equivalent.

**E. The case of a small central body $R_* < R_*^{\text{MCP}}$
in the canonical ensemble: Multirotations**

For a small central body $R_* < R_*^{\text{MCP}}$, the system can display both microcanonical and canonical phase transitions (zeroth and first order). The microcanonical caloric curve has been described in Sec. III A. Let us describe the corresponding caloric curve in the canonical ensemble. The series of

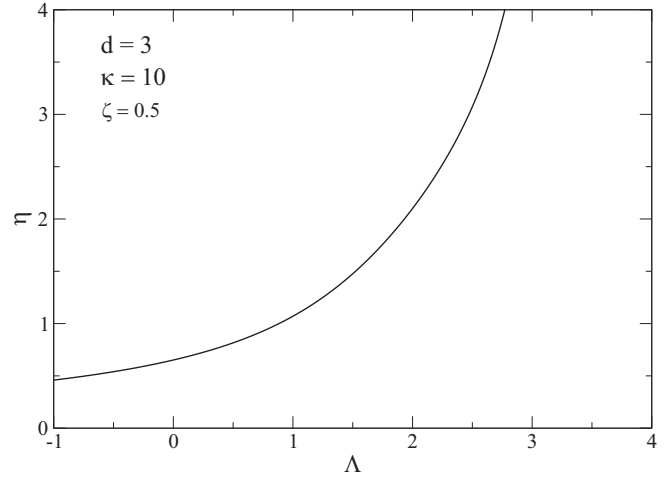


FIG. 15. Caloric curve for $\kappa = 10$ and $\zeta = 0.5 > \zeta_{\text{CCP}}$. It is monotonic and the ensembles are equivalent.

equilibria displays several turning points of temperature (see Fig. 16). At the first turning point T_c , the curve rotates clockwise so that a mode of stability is lost. At the second turning point of temperature, another mode of stability is lost. At the third turning point of temperature, the curve rotates anticlockwise so that the second mode is regained and at the fourth turning point of temperature T_* the first mode is regained.¹⁶ Therefore, the left branch (before T_c) and the right branch (after T_*) are canonically stable (free-energy minima) and form the physical canonical caloric curve. Although the structure of the series of equilibria in the unstable domain is more complex than in Sec. III B, because it displays several rotations, the

¹⁶We note that certain equilibrium states, deep in the spiral, are unstable in the canonical ensemble (and also in the microcanonical ensemble) although they have a positive specific heat (see footnotes 14 and 15).

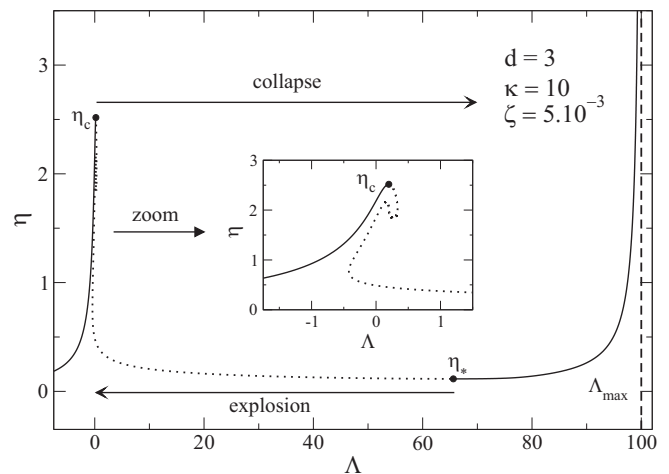


FIG. 16. Physical canonical caloric curve for $\zeta = 5 \times 10^{-3} < \zeta_{\text{MCP}}$ and $\kappa = 10$. The dotted lines represent the unstable states (saddle points).

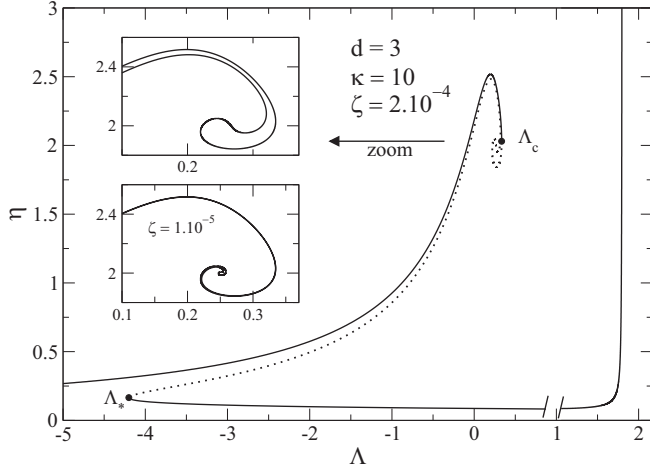


FIG. 17. Series of equilibria at fixed $\kappa = 10$ for several small values of ζ . As $\zeta \rightarrow 0$, the series of equilibria makes more and more rotations around the singular sphere $(\Lambda, \eta) = (1/4, 2)$ before unwinding (see inset). When $\zeta = 0$, we recover the classical spiral of a spherical isothermal self-gravitating system.

caloric curve corresponding to the stable part of the series of equilibria is simple and similar to Fig. 11 obtained for a larger value of the core radius. The strict canonical caloric curve containing only fully stable states (global free-energy minima) would also be similar to Fig. 14.

F. The limit of a vanishing central body $R_* \rightarrow 0$

It is of interest to study the limit of a vanishing central body $R_* \rightarrow 0$ to make the connection with the classical studies of Antonov [9], Lynden-Bell and Wood [15], and Katz [41].

As the radius of the central body decreases, the series of equilibria winds up several times before unwinding so that more and more turning points of energy and temperature appear. This is illustrated in Figs. 17 and 18. However, the discussion concerning the phase transitions remains essentially unchanged. In the microcanonical ensemble, the gaseous phase (upper branch) is stable until the energy E_c and the condensed phase (lower branch) is stable from the energy E_* . In the canonical ensemble, the gaseous phase (left branch) is stable until the temperature T_c and the condensed phase (right branch) is stable from the temperature T_* . When $R_* \rightarrow 0$, the energy $E_* \rightarrow -\infty$ and the temperature $T_* \rightarrow +\infty$. Similarly, $E_t \rightarrow -\infty$ and $T_t \rightarrow +\infty$. Therefore, the gaseous branch only contains metastable states. The condensed branch in the microcanonical ensemble approaches the $\beta = 0$ axis and is formed by configurations presenting a thin cusp containing a weak mass but a large potential energy surrounded by a hot and massive halo (in the absence of a central body, the gravothermal catastrophe leads to a tight binary star surrounded by a very hot halo with a very large entropy). The condensed branch in the canonical ensemble is rejected to $E \rightarrow -\infty$ and is formed by configurations presenting a thin cusp containing most of the mass (in the absence of a central body, the isothermal collapse leads to a Dirac peak containing all the mass and having a very negative free energy). The unstable branch makes several oscillations and leads to the

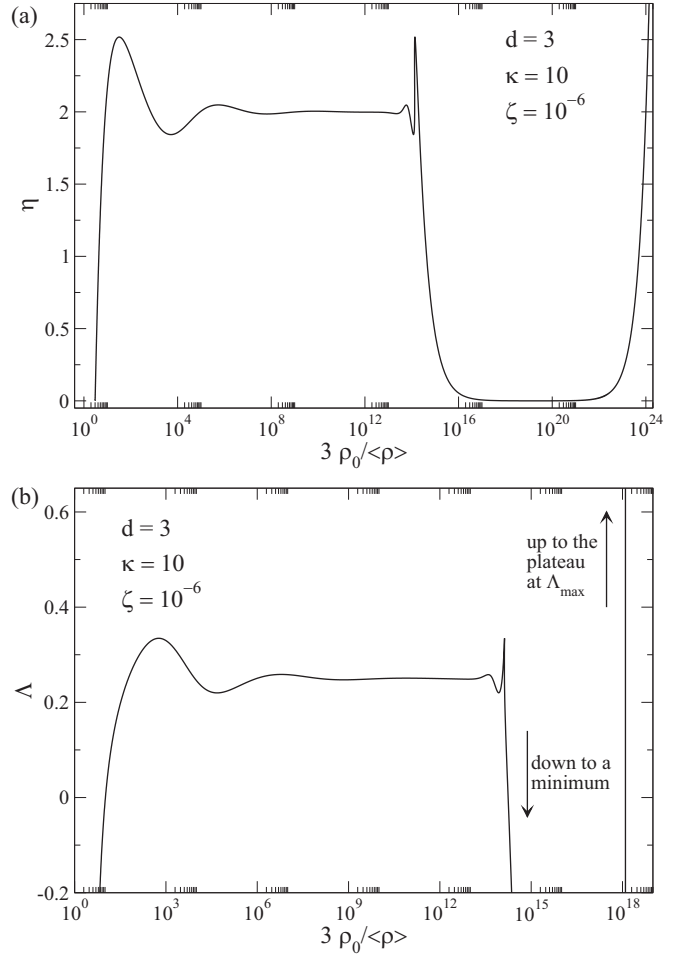


FIG. 18. Evolution of the energy Λ and inverse temperature η as a function of the normalized central density $\rho_0 / \langle \rho \rangle$.

classical spiral discussed by Antonov [9], Lynden-Bell and Wood [15], and Katz [41].

G. Critical points

The deformation of the series of equilibria as a function of the core radius R_* (for a fixed density ρ_* of the central body) is represented in Figs. 19 and 20. There are two critical points in the problem, one in each ensemble. When $R_* < R_*^{\text{MCP}}$, the series of equilibria $\beta(E)$ presents turning points of energy and temperature so that there exist phase transitions in the microcanonical and canonical ensembles. We have seen that the first-order phase transitions may not take place in practice due to the long lifetime of the metastable states. However, there remains zeroth order phase transitions associated with the gravothermal catastrophe in the microcanonical ensemble and the isothermal collapse in the canonical ensemble. Since the domains of stability differ in the canonical and microcanonical ensembles, the ensembles are not equivalent. Indeed, some states are stable (i.e., accessible) in the microcanonical ensemble while they are unstable (i.e., inaccessible) in the canonical ensemble. Since canonical stability implies microcanonical stability [94], the microcanonical ensemble contains more stable states than the canonical one. At the

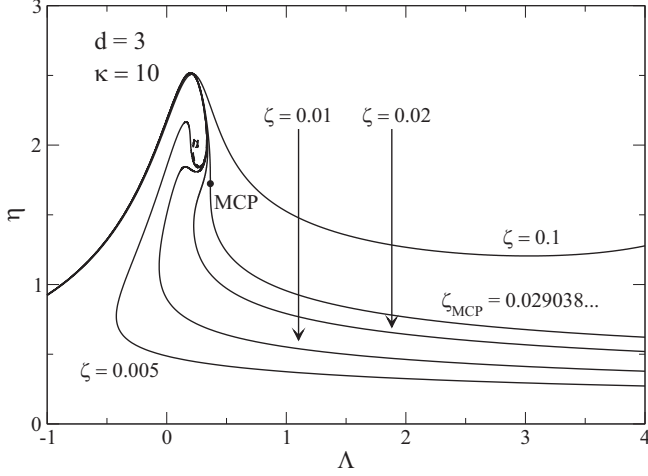


FIG. 19. Enlargement of the series of equilibria near the microcanonical critical point. When $\zeta = \zeta_{\text{MCP}}$, the curve $\eta(\Lambda)$ presents an inflexion point and the microcanonical phase transition (gravothermal catastrophe) is suppressed.

microcanonical critical point $R_* = R_*^{\text{MCP}}$, the series of equilibria $\beta(E)$ presents an inflexion point so that the microcanonical phase transition (gravothermal catastrophe) is suppressed (see Fig. 19). When $R_*^{\text{MCP}} < R_* < R_*^{\text{CCP}}$, the series of equilibria $\beta(E)$ presents turning points of temperature but no turning point of energy. Therefore, there exist phase transitions in the canonical ensemble but not in the microcanonical ensemble. The ensembles are not equivalent as revealed by the region of negative specific heat in the microcanonical ensemble that is replaced by a phase transition in the canonical ensemble. At the canonical critical point $R_* = R_*^{\text{CCP}}$, the series of equilibria $E(\beta)$ presents an inflexion point so that the canonical phase transition (isothermal collapse) is suppressed (see Fig. 20). When $R_* > R_*^{\text{CCP}}$, the series of equilibria $\beta(E)$ is monotonic

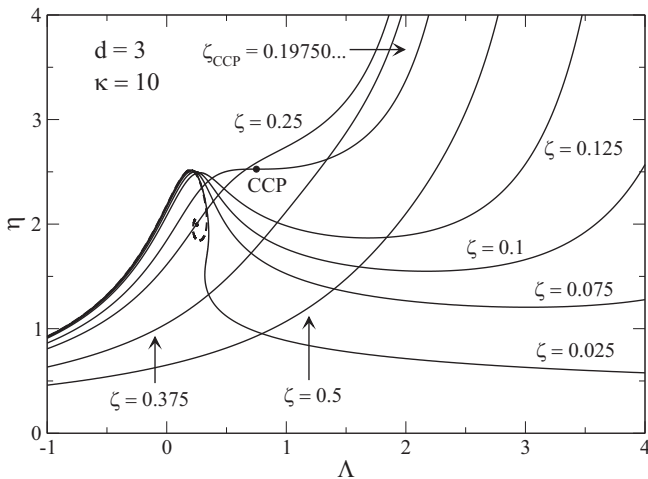


FIG. 20. Enlargement of the series of equilibria near the canonical critical point. When $\zeta = \zeta_{\text{CCP}}$, the curve $\Lambda(\eta)$ presents an inflexion point and the canonical phase transition (isothermal collapse) is suppressed.

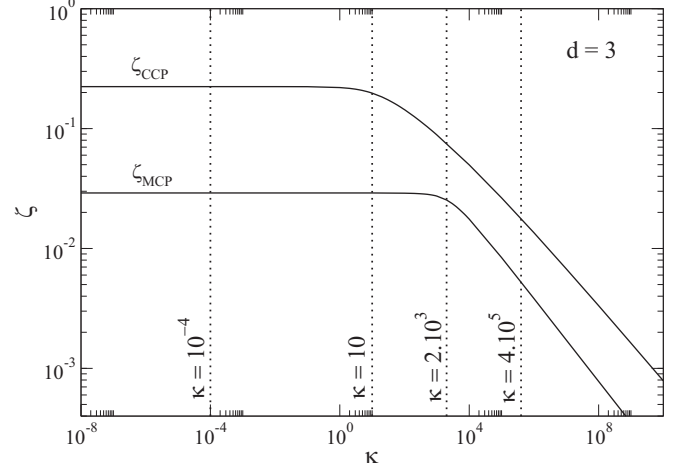


FIG. 21. Dependence of the microcanonical and canonical critical points ζ_{MCP} and ζ_{CCP} with the density of the central body κ . We have indicated for reference the values of κ that have been selected to construct the phase diagrams of Sec. III H (see Figs. 22 and 23 below).

so that there is no phase transition. In that case, the statistical ensembles are equivalent.

The values of the microcanonical and canonical critical points $R_*^{\text{MCP}}(\rho_*)$ and $R_*^{\text{CCP}}(\rho_*)$ depend on the density ρ_* of the central body. This dependence is represented in Fig. 21. At sufficiently large densities, the critical radii $R_*^{\text{MCP}}(\rho_*)$ and $R_*^{\text{CCP}}(\rho_*)$ decrease algebraically as $\rho_*^{-\alpha}$ with an exponent $\alpha \sim 0.3$.

H. Canonical and microcanonical phase diagrams

Typical curves illustrating canonical and microcanonical phase transitions are represented in Figs. 11 and 6, respectively. The phase diagrams of an isothermal gas with a central body can be directly obtained from these curves by identifying characteristic energies and characteristic temperatures.

In the canonical ensemble (see Fig. 11), where T is the control parameter, we note T_c (collapse temperature) the terminal point of the metastable gaseous phase (first turning point of temperature), and T_* (temperature of explosion) the terminal point of the metastable condensed phase (last turning point of temperature). These are the canonical spinodal points. The canonical phase diagram (R_*, T) is represented in Fig. 22 for different values of the density ρ_* of the central body. For $T > T_*$, the system is in the gaseous phase and for $T < T_c$ the system is in the condensed phase. For $T_* < T < T_c$ it can be in one of these two phases (as a stable or a metastable state) depending on the way it has been prepared. This is the region where hysteretic effects take place. The two characteristic temperatures T_c and T_* merge at the canonical critical point $R_* = R_*^{\text{CCP}}$. The strict phase diagram should exhibit the transition temperature T_t corresponding to the first-order phase transition (see Ref. [5] for self-gravitating fermions). However, since this phase transition does not take place in practice, we have only represented the physical phase diagram.

In the microcanonical ensemble (see Fig. 6), where E is the control parameter, we note E_c (collapse energy) the end

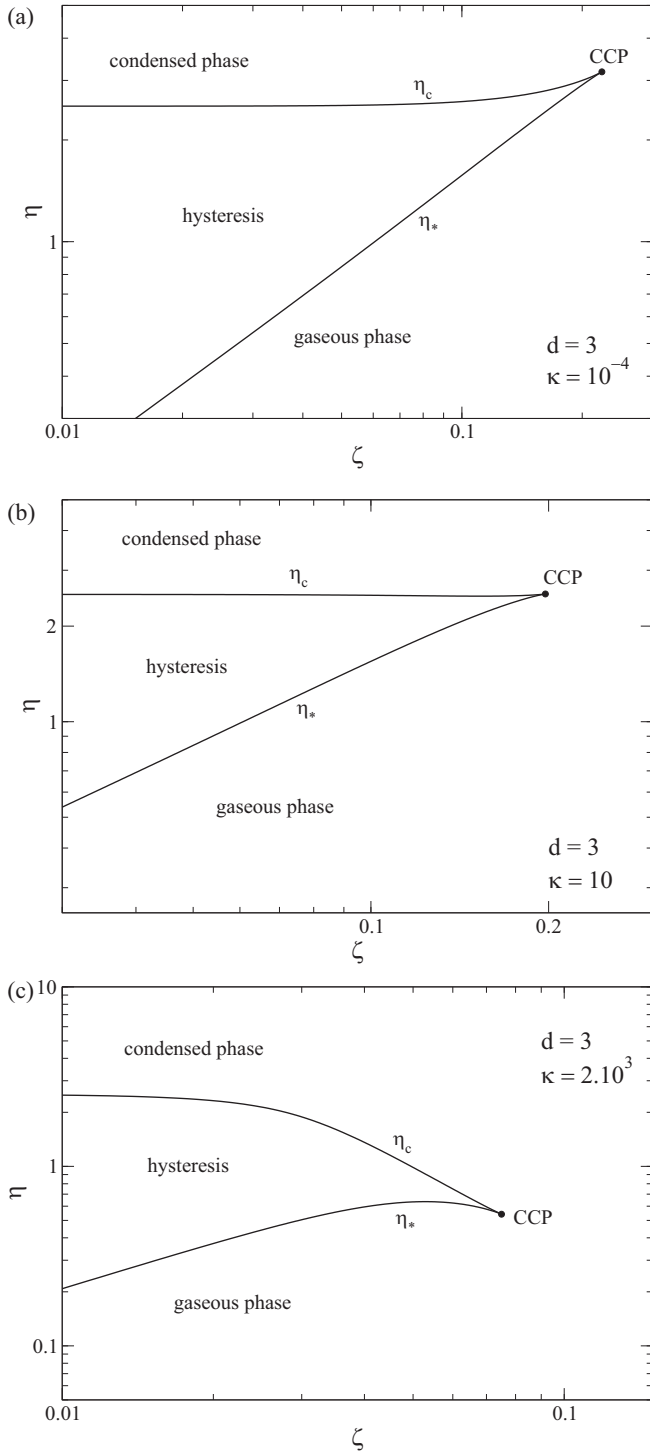


FIG. 22. Canonical phase diagrams in the (ζ, η) plane for different values of the parameter κ indicated in Fig. 21 (the canonical phase diagram for $\kappa = 4 \times 10^5$ is similar to the one for $\kappa = 2 \times 10^3$ so it is not represented). The region delimited by η_c and η_* corresponds to an hysteretic zone where the actual phase of the system depends on its history. If the system is initially prepared in a gaseous state, then it will remain gaseous until the minimum temperature $1/\eta_c$, at which it will collapse and become condensed. Inversely, if the system is initially prepared in a condensed state, then it will remain condensed until the maximum temperature $1/\eta_*$, at which it will explode and become gaseous.

point of the metastable gaseous phase (first turning point of energy), and E_* (energy of explosion) the end point of the metastable condensed phase (last turning point of energy). These are the microcanonical spinodal points. We also note E_{\min} the minimum energy. The microcanonical phase diagram (R_*, E) is represented in Fig. 23 for different values of the density ρ_* of the central body. For $E > E_*$, the system is in the gaseous phase and for $E_{\min} < E < E_c$ the system is in the condensed phase. For $E_* < E < E_c$ it can be in one of these two phases (as a stable or a metastable state) depending on the way it has been prepared. This is the region where hysteretic effects take place. The two characteristic energies E_c and E_* merge at the microcanonical critical point $R_* = R_*^{\text{MCP}}$. To complete the diagram, we have also denoted E_{gas} the energy at which we enter in the region of negative specific heats (first turning point of temperature) and E_{cond} the energy at which we leave the region of negative specific heats (last turning point of temperature), see Fig. 10. These two characteristic energies E_{gas} and E_{cond} merge at the canonical critical point $R_* = R_*^{\text{CCP}}$. The strict phase diagram should exhibit the transition energy E_t corresponding to the first-order phase transition (see Ref. [5] for self-gravitating fermions). However, since this phase transition does not take place in practice, we have only represented the physical phase diagram.

We note that the microcanonical phase diagram is richer than the canonical phase diagram due to the existence of a negative specific heat region. We recall that canonical stability implies microcanonical stability but the converse is false in case of ensemble inequivalence [94]. Therefore, canonical stability is a sufficient but not necessary condition of microcanonical stability. Since canonical equilibria are always realized as microcanonical equilibria, they constitute a subdomain of the microcanonical phase diagram. In particular, the states with energy between E_{gas} and E_{cond} , that have negative specific heats, are not accessible in the canonical ensemble (they are unstable saddle points of free energy) while they are accessible in the microcanonical ensemble (they are entropy maxima at fixed mass and energy). Therefore, this region corresponds to a domain of ensemble inequivalence.

I. The case of a denser and denser central body and the case of a central Dirac mass

We consider how the series of equilibria changes when the radius of the central body R_* is fixed and its mass M_* is progressively increased so that the density ρ_* of the central body is larger and larger. The series of equilibria are represented in Fig. 24. As the density ρ_* increases, the collapse temperature T_c and the collapse energy E_c increase, so that instability occurs sooner. Typical density profiles at the verge of the canonical instability ($T = T_c$) are represented in Fig. 25. The cusp is more and more pronounced as the density of the central body increases.

Finally, we consider the case where the mass M_* of the central body is fixed and its radius R_* is progressively reduced. The corresponding caloric curves are plotted in Fig. 26. For $R_* \rightarrow 0$, the central body tends to a Dirac mass. However, we know from Sec. II G that there is no equilibrium state in that case in $d = 3$. This is why the caloric curves do not tend to a well-defined limit for $R_* \rightarrow 0$.

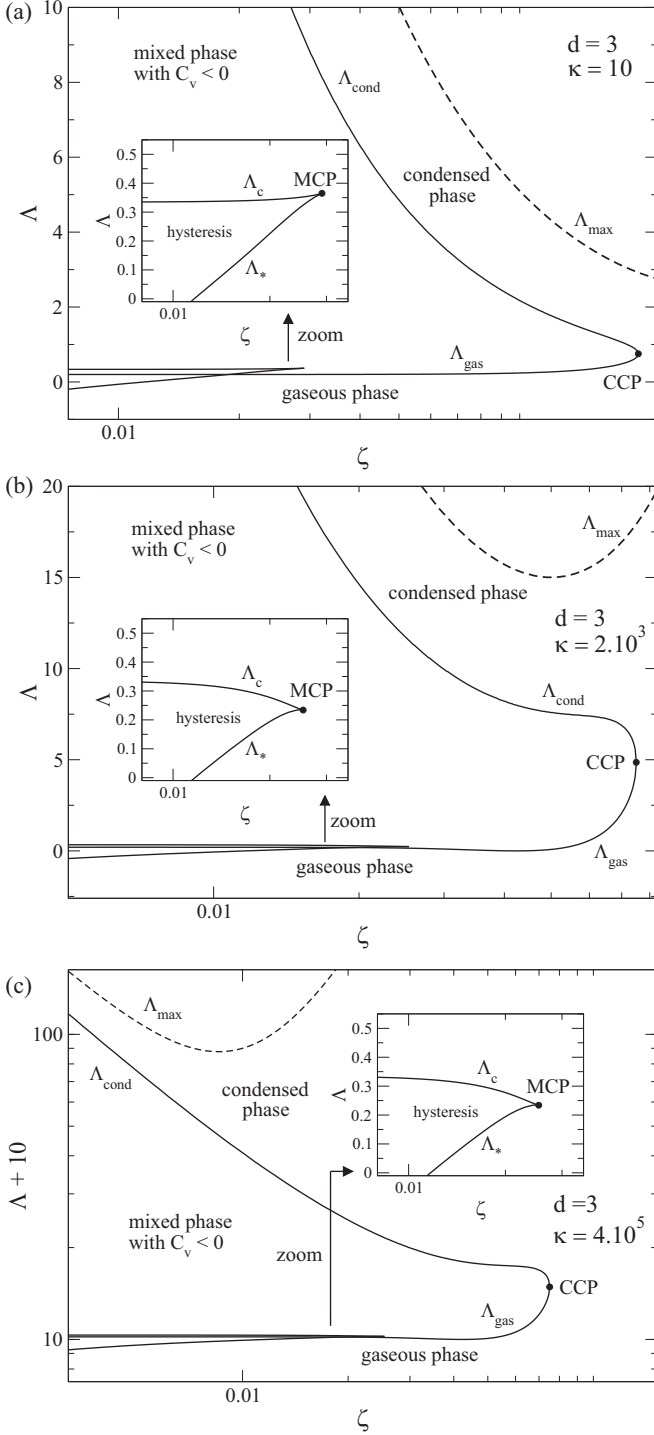


FIG. 23. Microcanonical phase diagrams in the (ζ, Λ) plane for different values of the parameter κ indicated in Fig. 21 (the microcanonical phase diagram for $\kappa = 10^{-4}$ is similar to the one for $\kappa = 10$ so it is not represented). The region delimited by Λ_c and Λ_* corresponds to an hysteretic zone where the actual phase of the system depends on its history. If the system is initially prepared in a gaseous state, then it will remain gaseous until the minimum energy $-\Lambda_c$, at which it will collapse and become condensed. Inversely, if the system is initially prepared in a condensed state, then it will remain condensed until the maximum energy $-\Lambda_*$, at which it will explode and become gaseous.

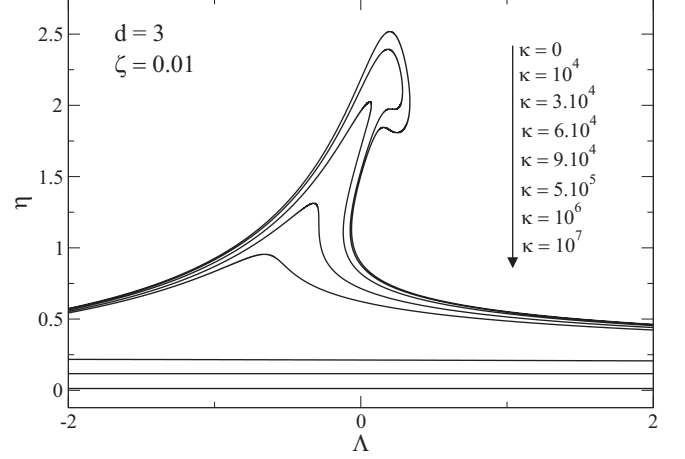


FIG. 24. Deformation of the series of equilibria as we progressively increase the density κ of the central body for a fixed value of the core radius $\zeta = 0.01$.

IV. CALORIC CURVES IN THE PRESENCE OF A CENTRAL BODY IN $d = 2$ AND $d = 1$ DIMENSIONS

In this section, we briefly describe the caloric curves of a classical isothermal self-gravitating gas in the presence of a central body in $d = 2$ and $d = 1$ dimensions. These caloric curves and the corresponding density profiles can be obtained analytically [90]. In the figures, we fix the mass M_* of the central body and decrease its radius R_* , approaching thereby a central Dirac mass when $R_* \rightarrow 0$.¹⁷

We consider only box-confined systems and refer to Ref. [90] for complementary results.

¹⁷In the biological problem, which is particularly justified in $d = 1$ and $d = 2$ dimensions (see Appendix A), it is more relevant to fix the mass of the chemoattractant rather than its density.

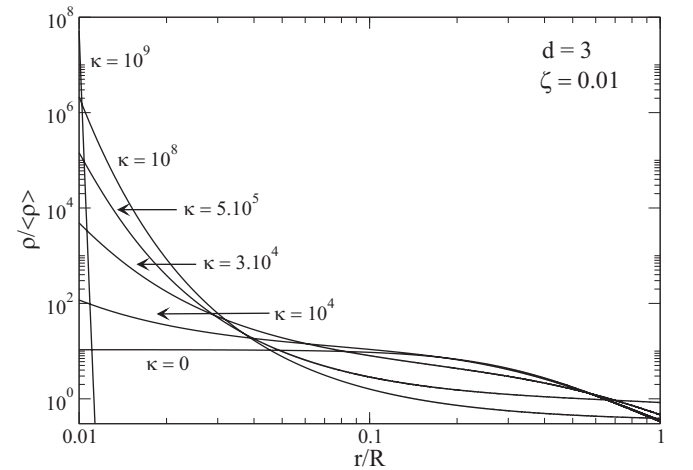


FIG. 25. Density profiles corresponding to the critical temperature $\eta = \eta_c$ as one increases the density of the central body. As κ increases, the self-gravitating particles are more and more condensed around the central body.

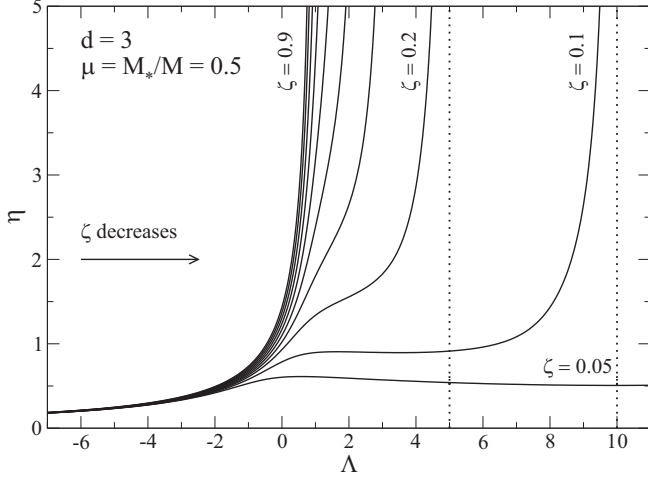


FIG. 26. Caloric curves at fixed central mass μ (we have taken $\mu = 0.5$ for illustration) for several values of the central body radius ζ . The case $\zeta \rightarrow 0$ corresponds to a central Dirac mass for which there is no equilibrium state.

The caloric curve of a classical self-gravitating gas without central body in $d = 2$ dimensions has been discussed by Katz and Lynden-Bell [79] and Sire and Chavanis [38]. The caloric curve $\beta(E)$ is monotonic (which implies thermodynamical stability) but the temperature tends to a constant $k_B T_c = GMm/4$ when $E \rightarrow -\infty$. Stable equilibrium state exists for all energies E in the microcanonical ensemble, but only for temperatures $T > T_c$ in the canonical ensemble. For $T \leq T_c$ the system collapses and ultimately forms a Dirac peak containing all the mass [38]. In the presence of a central body, the caloric curve is plotted in Fig. 27. There is a minimum energy E_{\min} at which the gas is concentrated on the surface of the solid body (see Appendix F). A stable equilibrium state exists for all energies $E \geq E_{\min}$ in the microcanonical ensemble and for all temperatures $T \geq 0$ in the canonical ensemble. As R_* decreases, the minimum energy E_{\min} is pushed toward more

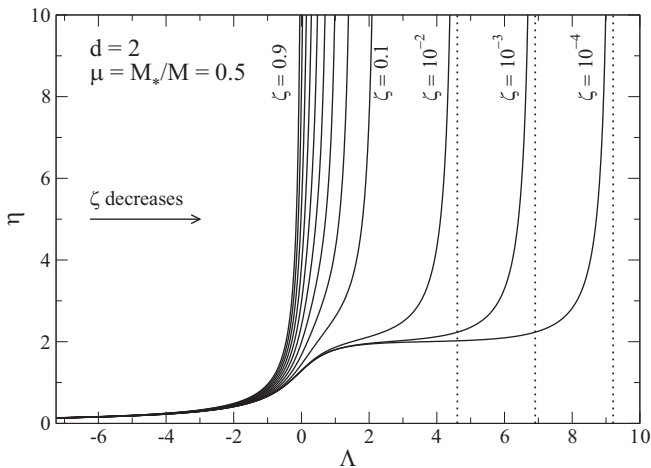


FIG. 27. Caloric curves at fixed central mass μ (we have taken $\mu = 0.5$ for illustration) for several values of the central body radius ζ . For small ζ (corresponding to a central Dirac mass), one observes the appearance of the critical temperature $\eta_c = 4/(1 + 2\mu) = 2$.

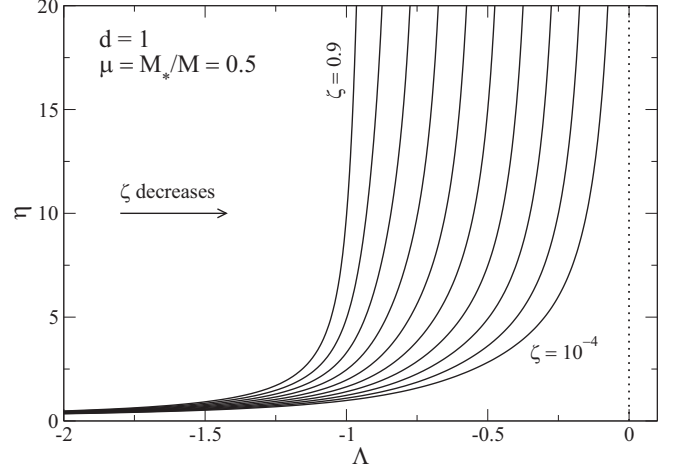


FIG. 28. Caloric curves at fixed central mass μ (we have taken $\mu = 0.5$ for illustration) for several values of the central body radius ζ . For small ζ (corresponding to a central Dirac mass), the minimum energy approaches the absolute minimum value $\Lambda = 0$.

and more negative values and a plateau forms at a critical temperature $k_B T_c = (GMm/4)(1 + 2M_*/M)$ modified by the presence of the central Dirac mass M_* [90]. These results are similar to those obtained for a Fermi gas in $d = 2$ dimensions [55,86,88].

The caloric curve of a classical self-gravitating gas without central body in $d = 1$ dimension has been discussed by Katz and Lecar [80] and Sire and Chavanis [38]. The caloric curve $\beta(E)$ is monotonic (which implies thermodynamical stability). Stable equilibrium state exists for all accessible energies $E \geq 0$ in the microcanonical ensemble, and for all temperatures $T \geq 0$ in the canonical ensemble. There are no mechanical instabilities. In the presence of a central body, the caloric curve is plotted in Fig. 28. There is a minimum energy $E_{\min} > 0$ at which the gas is concentrated on the surface of the solid body (see Appendix F). A stable equilibrium state exists for all energies $E \geq E_{\min}$ in the microcanonical ensemble, and for all temperatures $T \geq 0$ in the canonical ensemble. As R_* decreases, the minimum energy is pushed toward $E = 0$. These results are similar to those obtained for a Fermi gas in $d = 1$ [55,86,88].

V. CONCLUSION

In this work, we have studied the statistical equilibrium states of a classical self-gravitating gas around a central body. The central body can represent a planetary core or mimic a black hole at the center of a galaxy or at the center of a globular cluster. The gas is described by the Boltzmann distribution which is the fundamental distribution function predicted by statistical mechanics. Like in previous studies, we must enclose the system within a box to have a well-defined equilibrium (maximum entropy state). Otherwise, the gas evaporates and there is no statistical equilibrium state in a strict sense.

We have studied the phase transitions of this system in both microcanonical (fixed energy) and canonical (fixed temperature) ensembles in different dimensions of space. In $d = 3$

dimensions, and for sufficiently large systems, we have evidenced both microcanonical and canonical phase transitions. Below a critical energy in the microcanonical ensemble the atmosphere experiences a gravothermal catastrophe and below a critical temperature in the canonical ensemble it experiences an isothermal collapse. In the presence of a central body, the collapse stops when the gas comes into contact with the central body and forms a thin layer (spike) around it. This leads to a zeroth order phase transition between a dilute (gaseous) phase and a condensed phase with a “cusp-halo” structure. For intermediate-size systems, there are only canonical phase transitions (of zeroth order) and for small systems there is no phase transition at all. In $d = 2$ dimensions, there is no phase transition in a strict sense (no discontinuity of any thermodynamical parameter) but, for sufficiently large systems, a plateau temperature indicates a rapid change between a dilute phase and a condensed phase. In $d = 1$ dimension, there is no phase transition. In $d = 3$ dimensions there are regions of ensemble inequivalence (except for small systems) associated with negative specific heats while in $d = 2$ and $d = 1$ dimensions the specific heat is positive and the ensembles are equivalent. These results are similar to those obtained previously for self-gravitating fermions [5]. There is, however, a structural difference. In the case of fermions, the small-scale regularization is intrinsic to the quantum system (it arises from the Pauli exclusion principle contained in the Fermi-Dirac distribution) while, in the present case, the distribution function is classical and the small-scale regularization is external to the system (it is due to the finite radius of the central body).

Of course, the box is artificial and we can have two points of view on this problem. If we are mainly interested in statistical mechanics, then it is relevant to use the Boltzmann distribution (which is the fundamental distribution function of statistical mechanics) and introduce a box to make the problem well-defined mathematically. In this sense, our thermodynamic approach is rigorously justified. If we are rather interested in astrophysical applications, then we can use a truncated Boltzmann distribution, e.g., the King [29] distribution, to take into account the evaporation of the particles and avoid the artificial box. Although we gain in realism, the problem becomes less well-justified from a statistical mechanics point of view because we now have to deal with an out-of-equilibrium problem. We can nevertheless try to apply a thermodynamical approach as discussed by Katz [30] and Chavanis *et al.* [31] for the classical King model. The study of phase transitions in the fermionic King model [97,98] has been performed in Refs. [70,71] both for nonrelativistic and relativistic systems, giving results qualitatively similar to those obtained in a box [5,68,69]. Recently, Bonsor *et al.* [99] have considered the equilibrium states of a loaded King distribution around a central body. In this study, the central body models a black hole at the center of a globular cluster. They report a transition between equilibria which are dominated by the mass of the host stellar system or by the mass of the central black hole. Their results are complementary to those obtained for the classical and fermionic King models studied in Refs. [31,70] and for the box-confined classical isothermal gas surrounding a central body considered in the present article. These works provide a rather complete picture of gravitational phase transitions in these different contexts.

APPENDIX A: ANALOGY BETWEEN SELF-GRAVITATING SYSTEMS AND BACTERIAL POPULATIONS

In this Appendix, we point out some analogies between a gas of self-gravitating Brownian particles [37–39] and the chemotaxis of bacterial populations [72,73] (see, e.g., Refs. [74,85,100–105] for more details on this analogy). The name chemotaxis refers to the motion of organisms induced by chemical signals. In some cases, the biological organisms secrete a substance (chemoattractant, pheromone) that has an attractive effect on the organisms themselves. Therefore, in addition to their diffusive motion, they move systematically along the gradient of concentration of the chemical they secrete (chemotactic flux). When attraction prevails over diffusion, the chemotaxis can trigger a self-accelerating process (chemotactic collapse) until a point at which aggregation takes place. This is the case for the slime mold *Dictyostelium discoideum* and for the bacteria *Escherichia coli*. The Keller-Segel [106] model describing the chemotaxis of biological populations can be written as

$$\frac{\partial \rho}{\partial t} = \nabla \cdot (D \nabla \rho - \chi \rho \nabla c), \quad (\text{A1})$$

$$\frac{1}{D'} \frac{\partial c}{\partial t} = \Delta c - k^2 c + \lambda \rho, \quad (\text{A2})$$

where $\rho(\mathbf{r}, t)$ is the concentration of the biological species (e.g., bacteria) and $c(\mathbf{r}, t)$ is the concentration of the secreted chemical. The bacteria diffuse with a diffusion coefficient D and undergo a chemotactic drift with strength χ along the gradient of chemical. The chemical is produced by the bacteria at a rate $D'\lambda$, is degraded at a rate $D'k^2$, and diffuses with a diffusion coefficient D' . In the limit of large diffusivity of the chemical $D' \rightarrow +\infty$ and a vanishing degradation rate $k^2 = 0$, the reaction-diffusion equation (A2) reduces to the Poisson equation $\Delta c = -\lambda \rho$ (see Appendix C of Ref. [101] for more details). In that case, the Keller-Segel model becomes isomorphic to the Smoluchowski-Poisson equations describing self-gravitating Brownian particles in a high friction limit $\xi \rightarrow +\infty$ [37–39]:

$$\xi \frac{\partial \rho}{\partial t} = \nabla \cdot \left(\frac{k_B T}{m} \nabla \rho + \rho \nabla \Phi \right), \quad (\text{A3})$$

$$\Delta \Phi = S_d G \rho. \quad (\text{A4})$$

In this analogy, the concentration of chemical $c(\mathbf{r}, t)$, plays the role of minus the gravitational potential $-\Phi(\mathbf{r}, t)$. The effective statistical ensemble associated with the Keller-Segel model is the canonical ensemble.¹⁸ The steady states of the Keller-Segel model are of the form $\rho = A e^{(\chi/D)c}$ which is similar to the Boltzmann distribution $\rho = A e^{-\beta m \Phi}$ with an effective temperature $T_{\text{eff}} = D/\chi$ given by a form of Einstein relation. The Lyapunov functional associated with the Keller-Segel model is $F = -\frac{1}{2} \int \rho c \, d\mathbf{r} + \frac{D}{\chi} \int \rho \ln \rho \, d\mathbf{r}$. It is similar to a free energy $F = E - TS$ in thermodynamics, where E is the energy and S is the Boltzmann entropy. The Keller-Segel

¹⁸The drift-diffusion equation (A1) and the Smoluchowski equation (A3) can be interpreted as Fokker-Planck equations in position space describing an overdamped dynamics. In the Brownian picture, the particles are in contact with a heat bath fixing the temperature.

model conserves the mass and satisfies an H -theorem for the free energy, i.e., $\dot{F} \leq 0$ with an equality if, and only if, ρ is the Boltzmann distribution discussed above. Furthermore, the Boltzmann distribution is dynamically stable if, and only if, it is a local minimum of free energy at fixed mass. In that context, the minimization problem $\min_{\rho} \{F[\rho] | M[\rho] = M\}$ determines a steady state of the Keller-Segel model that is dynamically stable. This is similar to a condition of thermodynamical stability in the canonical ensemble.

Remark. There also exist remarkable analogies between the statistical mechanics of self-gravitating systems and two-dimensional point vortices (see the contribution of P.H. Chavanis in Ref. [6]). The analogy between self-gravitating systems, bacterial populations and two-dimensional point vortices (with a detailed list of references) is further discussed in Appendix A of Ref. [90].

APPENDIX B: THE VIRIAL THEOREM

In this Appendix we derive the equilibrium scalar virial theorem for a self-gravitating system in the presence of a central body in d dimensions. We refer to Appendix G of Ref. [107] and Appendix B of Ref. [108] for more details and generalizations.

1. The virial of the gravitational force produced by the central body

Assuming that the central body is spherically symmetric, and using Newton's law (see Appendix D), the gravitational field that it creates in $r \geq R_*$ is

$$-\nabla \Phi_{\text{ext}} = -\frac{GM_*}{r^{d-1}} \mathbf{e}_r \quad \text{or} \quad \frac{d\Phi_{\text{ext}}}{dr} = \frac{GM_*}{r^{d-1}}. \quad (\text{B1})$$

In particular, we have

$$\frac{d\Phi_{\text{ext}}}{dr}(R_*) = \frac{GM_*}{R_*^{d-1}}. \quad (\text{B2})$$

The corresponding gravitational potential in $r \geq R_*$ is

$$\Phi_{\text{ext}} = -\frac{1}{d-2} \frac{GM_*}{r^{d-2}} \quad (d \neq 2), \quad (\text{B3})$$

$$\Phi_{\text{ext}} = GM_* \ln\left(\frac{r}{R}\right) \quad (d = 2). \quad (\text{B4})$$

This is the solution of the Laplace equation

$$\Delta \Phi_{\text{ext}} = 0. \quad (\text{B5})$$

The gravitational energy of the gas in the potential created by the central body is

$$W_{\text{ext}} = \int \rho \Phi_{\text{ext}} d\mathbf{r}. \quad (\text{B6})$$

Using Eqs. (B3) and (B4) we get

$$W_{\text{ext}} = -\frac{1}{d-2} \int \rho \frac{GM_*}{r^{d-2}} d\mathbf{r} \quad (d \neq 2), \quad (\text{B7})$$

$$W_{\text{ext}} = GM_* \int \rho \ln\left(\frac{r}{R}\right) d\mathbf{r} \quad (d = 2). \quad (\text{B8})$$

The virial of the external force is defined by

$$W_{ii}^{\text{ext}} = - \int \rho \mathbf{r} \cdot \nabla \Phi_{\text{ext}} d\mathbf{r}. \quad (\text{B9})$$

Using Eq. (B1), we get

$$W_{ii}^{\text{ext}} = - \int \rho \frac{GM_*}{r^{d-2}} d\mathbf{r}. \quad (\text{B10})$$

For $d \neq 2$, comparing Eqs. (B7) and (B10) we find that

$$W_{ii}^{\text{ext}} = (d-2)W_{\text{ext}}. \quad (\text{B11})$$

For $d = 2$, Eq. (B10) yields

$$W_{ii}^{\text{ext}} = -GM_*M. \quad (\text{B12})$$

2. The virial of the gravitational force produced by the gas

The gravitational field produced by the gas is

$$-\nabla \Phi(\mathbf{r}) = -G \int \rho(\mathbf{r}') \frac{\mathbf{r} - \mathbf{r}'}{|\mathbf{r} - \mathbf{r}'|^d} d\mathbf{r}'. \quad (\text{B13})$$

The corresponding gravitational potential is

$$\Phi(\mathbf{r}) = -\frac{G}{d-2} \int \frac{\rho(\mathbf{r}')}{|\mathbf{r} - \mathbf{r}'|^{d-2}} d\mathbf{r}' \quad (d \neq 2), \quad (\text{B14})$$

$$\Phi(\mathbf{r}) = G \int \rho(\mathbf{r}') \ln \frac{|\mathbf{r} - \mathbf{r}'|}{R} d\mathbf{r}' \quad (d = 2). \quad (\text{B15})$$

This is the solution of the Poisson equation

$$\Delta \Phi = S_d G \rho. \quad (\text{B16})$$

The gravitational energy of the gas due to the interaction of the particles between themselves is

$$W = \frac{1}{2} \int \rho \Phi d\mathbf{r}. \quad (\text{B17})$$

Using Eqs. (B14) and (B15) we get

$$W = -\frac{1}{2} \frac{G}{d-2} \int \frac{\rho(\mathbf{r})\rho(\mathbf{r}')}{|\mathbf{r} - \mathbf{r}'|^{d-2}} d\mathbf{r}d\mathbf{r}' \quad (d \neq 2), \quad (\text{B18})$$

$$W = \frac{1}{2} G \int \rho(\mathbf{r})\rho(\mathbf{r}') \ln \frac{|\mathbf{r} - \mathbf{r}'|}{R} d\mathbf{r}d\mathbf{r}' \quad (d = 2). \quad (\text{B19})$$

The virial of the gravitational force produced by the gas is

$$W_{ii} = - \int \rho \mathbf{r} \cdot \nabla \Phi d\mathbf{r}. \quad (\text{B20})$$

Substituting Eq. (B13) into Eq. (B20), we get

$$W_{ii} = -G \int \rho(\mathbf{r})\rho(\mathbf{r}') \frac{\mathbf{r} \cdot (\mathbf{r} - \mathbf{r}')}{|\mathbf{r} - \mathbf{r}'|^d} d\mathbf{r}d\mathbf{r}'. \quad (\text{B21})$$

Interchanging the dummy variables \mathbf{r} and \mathbf{r}' and adding the resulting expression to Eq. (B21), we obtain

$$W_{ii} = -\frac{1}{2} G \int \frac{\rho(\mathbf{r})\rho(\mathbf{r}')}{|\mathbf{r} - \mathbf{r}'|^{d-2}} d\mathbf{r}d\mathbf{r}'. \quad (\text{B22})$$

For $d \neq 2$, comparing Eqs. (B18) and (B22) we find that

$$W_{ii} = (d-2)W. \quad (\text{B23})$$

For $d = 2$, Eq. (B22) yields

$$W_{ii} = -\frac{GM^2}{2}. \quad (\text{B24})$$

These results are valid for an arbitrary distribution of the particles of the gas. In particular, for $d \neq 2$, we have

$$W = -\frac{1}{d-2} \int \rho \mathbf{r} \cdot \nabla \Phi d\mathbf{r}. \quad (\text{B25})$$

Now, for a spherically symmetric system, according to Newton's law (see Appendix D), we have

$$-\nabla \Phi = -\frac{GM(r)}{r^{d-1}} \mathbf{e}_r \quad \text{or} \quad \frac{d\Phi}{dr} = \frac{GM(r)}{r^{d-1}}, \quad (\text{B26})$$

where

$$M(r) = \int_{R_*}^r \rho(r') S_d r'^{d-1} dr' \quad (\text{B27})$$

is the mass of the gas contained within the sphere of radius r . Using Eqs. (B26) and (B27), the virial of the gravitational force (B20) can be written as

$$W_{ii} = -S_d G \int_{R_*}^R \rho(r) M(r) r dr = -\int_{R_*}^R \frac{GM(r)}{r^{d-2}} dM(r). \quad (\text{B28})$$

For $d = 2$, we immediately recover Eq. (B24). For $d \neq 2$, using Eq. (B23), we obtain the formula

$$W = -\frac{1}{d-2} \int_{R_*}^R \rho(r) \frac{GM(r)}{r^{d-2}} S_d r^{d-1} dr, \quad (\text{B29})$$

which is useful to calculate the gravitational potential energy of a spherically symmetric distribution of matter. This expression can be directly obtained by approaching from infinity a succession of spherical shells of mass $dM(r) = \rho(r) S_d r^{d-1} dr$ with potential energy $-GM(r)dM(r)/[(d-2)r^{d-2}]$ in the field of the mass $M(r)$ already present, and integrating over r .

Remark. Combining Eqs. (59), (B7), and (B29) we get

$$W_{\text{tot}} = -\frac{1}{d-2} \int_{R_*}^R \rho(r) \frac{G[M_* + M(r)]}{r^{d-2}} S_d r^{d-1} dr \quad (\text{B30})$$

or, equivalently,

$$W_{\text{tot}} = -\frac{S_d G}{d-2} \int_{R_*}^R \rho(r) (M_* + M(r)) r dr. \quad (\text{B31})$$

3. The equilibrium virial theorem

The condition of hydrostatic equilibrium from Eq. (43) can be rewritten as

$$\nabla P + \rho \nabla \Phi + \rho \nabla \Phi_{\text{ext}} = \mathbf{0}. \quad (\text{B32})$$

Taking the scalar product of this relation with \mathbf{r} and integrating over the region containing the gas we get

$$\int \mathbf{r} \cdot \nabla P d\mathbf{r} - W_{ii} - W_{ii}^{\text{ext}} = 0, \quad (\text{B33})$$

where W_{ii}^{ext} and W_{ii} are defined by Eqs. (B9) and (B20). Integrating by parts, we obtain the scalar virial theorem

$$d \int P d\mathbf{r} + W_{ii} + W_{ii}^{\text{ext}} = \oint \mathbf{Pr} \cdot d\mathbf{S}. \quad (\text{B34})$$

For a nonrelativistic gas, the local pressure is given by

$$P = \frac{1}{d} \int f v^2 d\mathbf{v}. \quad (\text{B35})$$

This relation is valid for an arbitrary distribution function. The kinetic energy is

$$E_{\text{kin}} = \int f \frac{v^2}{2} d\mathbf{r} d\mathbf{v}. \quad (\text{B36})$$

Therefore, we have the relation

$$E_{\text{kin}} = \frac{d}{2} \int P d\mathbf{r}. \quad (\text{B37})$$

The scalar virial theorem can then be rewritten as

$$2E_{\text{kin}} + W_{ii} + W_{ii}^{\text{ext}} = \oint \mathbf{Pr} \cdot d\mathbf{S}. \quad (\text{B38})$$

For $d \neq 2$, using Eqs. (B11) and (B23) we obtain

$$2E_{\text{kin}} + (d-2)W_{\text{tot}} = \oint \mathbf{Pr} \cdot d\mathbf{S}, \quad (\text{B39})$$

where we have introduced $W_{\text{tot}} = W + W_{\text{ext}}$. For $d = 2$, using Eqs. (B12) and (B24) we get

$$2E_{\text{kin}} - \frac{GM^2}{2} \left(1 + 2\frac{M_*}{M}\right) = \oint \mathbf{Pr} \cdot d\mathbf{S}. \quad (\text{B40})$$

To obtain these identities, we have not assumed that the gas is spherically symmetric (only that the central body is spherically symmetric). Now, for a spherically symmetric system enclosed between the spheres of radius R_* and R , owing to the fact that the pressure P is uniform on these spheres, we have

$$\oint \mathbf{Pr} \cdot d\mathbf{S} = d[P(R)V - P(R_*)V_*], \quad (\text{B41})$$

where V and V_* are the volumes of the spheres of radius R and R_* , respectively. Since $V = \frac{1}{d} S_d R^d$ this relation can be rewritten as

$$\oint \mathbf{Pr} \cdot d\mathbf{S} = P(R) S_d R^d - P(R_*) S_d R_*^d. \quad (\text{B42})$$

The scalar virial theorem is then given by Eqs. (B39) and (B40) with Eq. (B42).

APPENDIX C: CONDITION OF HYDROSTATIC EQUILIBRIUM FOR A SPHERICAL AND ISOTROPIC STELLAR SYSTEM

A self-gravitating gas is described by the Euler-Poisson equations

$$\frac{\partial \rho}{\partial t} + \nabla \cdot (\rho \mathbf{u}) = 0, \quad (\text{C1})$$

$$\frac{\partial \mathbf{u}}{\partial t} + (\mathbf{u} \cdot \nabla) \mathbf{u} = -\frac{1}{\rho} \nabla P - \nabla \Phi, \quad (\text{C2})$$

$$\Delta \Phi = S_d G \rho. \quad (\text{C3})$$

The condition of hydrostatic equilibrium expressing the balance between the pressure force and the gravitational force reads

$$\nabla P + \rho \nabla \Phi = \mathbf{0}. \quad (\text{C4})$$

For a barotropic gas, the pressure is a function $P = P(\rho)$ of the density.

A collisionless self-gravitating system is described by the Vlasov-Poisson equations

$$\frac{\partial f}{\partial t} + \mathbf{v} \cdot \frac{\partial f}{\partial \mathbf{r}} - \nabla \Phi \cdot \frac{\partial f}{\partial \mathbf{v}} = 0, \quad (\text{C5})$$

$$\Delta \Phi = S_d G \int f d\mathbf{v}. \quad (\text{C6})$$

The Vlasov-Poisson equations admit an infinite number of stationary states that are determined by the Jeans theorem [27,109]. When ‘‘collisions’’ (strong collisions or gravitational encounters) are taken into account, the right-hand side of Eq. (C5) is replaced by a collision term $C(f)$ of the Boltzmann, Landau, or Lenard-Balescu type, which tends to select the Boltzmann distribution among the infinite class of stationary solutions of the Vlasov equation (see, e.g., Ref. [91] for a detailed discussion on the kinetic theory of self-gravitating systems).

Let us consider a stellar system described by a distribution function $f(\mathbf{r}, \mathbf{v})$. For a spherical and isotropic system we have $f = f(\epsilon)$, where $\epsilon = v^2/2 + \Phi(\mathbf{r})$ is the individual energy of the stars by unit of mass. We define the density

$$\rho(\mathbf{r}) = \int f d\mathbf{v} = \int f[v^2/2 + \Phi(\mathbf{r})] d\mathbf{v} \quad (\text{C7})$$

and the pressure

$$P(\mathbf{r}) = \frac{1}{d} \int f v^2 d\mathbf{v} = \frac{1}{d} \int f[v^2/2 + \Phi(\mathbf{r})] v^2 d\mathbf{v}. \quad (\text{C8})$$

We note that $\rho(\mathbf{r}) = \rho[\Phi(\mathbf{r})]$ and $P(\mathbf{r}) = P[\Phi(\mathbf{r})]$ depend only on the gravitational potential. Eliminating formally $\Phi(\mathbf{r})$ between these two expressions, we find that the equation of state is barotropic in the sense that the pressure depends only on the density: $P(\mathbf{r}) = P[\rho(\mathbf{r})]$. We can therefore associate to the stellar system with distribution function $f(\epsilon)$ a corresponding barotropic gas with an equation of state $P = P(\rho)$. Taking the gradient of the pressure in Eq. (C8) and making straightforward manipulations, we get

$$\begin{aligned} \nabla P &= \frac{1}{d} \nabla \Phi \int f'(\epsilon) v^2 d\mathbf{v} \\ &= \frac{1}{d} \nabla \Phi \int \frac{\partial f}{\partial \mathbf{v}} \cdot \mathbf{v} d\mathbf{v} \\ &= -\frac{1}{d} \nabla \Phi \int f \nabla \cdot \mathbf{v} d\mathbf{v} \\ &= -\nabla \Phi \int f d\mathbf{v}. \end{aligned} \quad (\text{C9})$$

We therefore recover the condition of hydrostatic equilibrium for a gas

$$\nabla P + \rho \nabla \Phi = \mathbf{0}. \quad (\text{C10})$$

In the presence of an external potential Φ_{ext} , we just have to make the substitution $\Phi \rightarrow \Phi + \Phi_{\text{ext}}$.

APPENDIX D: NEWTON’S LAW IN d DIMENSIONS

If we consider a spherically symmetric distribution of matter with density $\rho(r)$, then the Poisson equation

$$\Delta \Phi = S_d G \rho \quad (\text{D1})$$

becomes

$$\frac{1}{r^{d-1}} \frac{d}{dr} \left(r^{d-1} \frac{d\Phi}{dr} \right) = S_d G \rho. \quad (\text{D2})$$

Integrating this equation between 0 and r , we obtain

$$\frac{d\Phi}{dr} = \frac{GM(r)}{r^{d-1}}, \quad (\text{D3})$$

where

$$M(r) = \int_0^r \rho(r') S_d r'^{d-1} dr' \quad (\text{D4})$$

denotes the mass contained within the sphere of radius r . We have

$$\rho(r) = \frac{M'(r)}{S_d r^{d-1}}. \quad (\text{D5})$$

Equation (D3) expresses Newton’s second theorem (in d dimensions) saying that the gravitational force produced in r by a spherically symmetric distribution of matter is the same as it would be if all the mass $M(r)$ were concentrated into a point at its center. In vectorial form,

$$-\nabla \Phi = -\frac{GM(r)}{r^{d-1}} \mathbf{e}_r. \quad (\text{D6})$$

This equation can also be obtained by integrating Eq. (D1) over a sphere of radius r and using the Gauss (or Ostrogradsky) theorem.

If the density $\rho(r)$ vanishes above a certain radius R , then for $r \geq R$, we have

$$\frac{d\Phi}{dr} = \frac{GM}{r^{d-1}}, \quad (\text{D7})$$

where $M = M(R)$ is the mass enclosed within the sphere of radius R . In particular, on the surface of the object, we obtain

$$\frac{d\Phi}{dr}(R) = \frac{GM}{R^{d-1}}. \quad (\text{D8})$$

For $r \geq R$, the gravitational potential is given by

$$\Phi(r) = -\frac{1}{d-2} \frac{GM}{r^{d-2}} \quad (d \neq 2), \quad (\text{D9})$$

$$\Phi(r) = GM \ln \left(\frac{r}{R} \right) \quad (d = 2). \quad (\text{D10})$$

In particular,

$$\Phi(R) = -\frac{1}{d-2} \frac{GM}{R^{d-2}} \quad (d \neq 2), \quad (\text{D11})$$

$$\Phi(R) = 0 \quad (d = 2). \quad (\text{D12})$$

APPENDIX E: THE POTENTIAL IN $d = 3$ DIMENSIONS FOR A SPHERICALLY SYMMETRIC SYSTEM

For a spherically symmetric system, the gravitational potential in $d = 3$ can be written as

$$\Phi(r) = -G \int_{R_*}^R \int_0^{2\pi} \int_0^\pi \frac{\rho(r_1)}{|\mathbf{r} - \mathbf{r}_1|} \sin \theta d\theta d\phi r_1^2 dr_1. \quad (\text{E1})$$

Introducing the expansion

$$\frac{1}{|\mathbf{r} - \mathbf{r}_1|} = \sum_{l=0}^{+\infty} \frac{r_{<}^l}{r_{>}^{l+1}} P_l(\cos \theta), \quad (\text{E2})$$

where $r_{<} = \min(r, r_1)$ and $r_{>} = \max(r, r_1)$ in Eq. (E1), making the change of variable $x = \cos \theta$ and using the identity $\int_{-1}^{+1} P_l(x) dx = 2\delta_{l0}$, we find that

$$\Phi(r) = -4\pi G \left[\frac{1}{r} \int_{R_*}^r \rho(r_1) r_1^2 dr_1 + \int_r^R \rho(r_1) r_1 dr_1 \right]. \quad (\text{E3})$$

From this expression, we get

$$\Phi(R_*) = -4\pi G \int_{R_*}^R \rho(r) r dr. \quad (\text{E4})$$

APPENDIX F: THE ENERGY OF THE GROUND STATE

At $T = 0$, all the gas is uniformly concentrated on the surface of the central body. Therefore, the energy of the ground state $E_{\min} = W_{\text{tot}}^{\min}$ corresponds to the potential energy

associated to this configuration. To compute this minimum energy, we start from Eq. (59). Accounting for the fact that the total mass of the gas M is located at $r = R_*$, we have

$$E_{\min} = \frac{1}{2} M \Phi(R_*) + \Phi_{\text{ext}}(R_*) M. \quad (\text{F1})$$

For $d \neq 2$, using Eqs. (B3) and (D9), we obtain

$$E_{\min} = -\frac{1}{d-2} (1 + 2\mu) \frac{GM^2}{R_*^{d-2}}. \quad (\text{F2})$$

The normalized minimum energy is therefore

$$\Lambda_{\max} = \frac{1 + 2\mu}{2(d-2)\zeta^{d-2}}. \quad (\text{F3})$$

For $d = 2$, using Eqs. (B4) and (D10), we obtain

$$E_{\min} = \frac{GM^2}{2} (1 + 2\mu) \ln \left(\frac{R_*}{R} \right). \quad (\text{F4})$$

The normalized minimum energy is therefore

$$\Lambda_{\max} = -\frac{1}{2} (1 + 2\mu) \ln \zeta. \quad (\text{F5})$$

-
- [1] T. Padmanabhan, *Phys. Rep.* **188**, 285 (1990).
[2] H. J. de Vega and N. Sanchez, *Nucl. Phys. B* **625**, 409 (2002).
[3] H. J. de Vega and N. Sanchez, *Nucl. Phys. B* **625**, 460 (2002).
[4] J. Katz, *Found. Phys.* **33**, 223 (2003).
[5] P. H. Chavanis, *Int. J. Mod. Phys. B* **20**, 3113 (2006).
[6] *Dynamics and Thermodynamics of Systems with Long-Range Interactions*, edited by T. Dauxois, S. Ruffo, E. Arimondo, and M. Wilkens, Lecture Notes in Physics (Springer, Berlin, 2002).
[7] A. Campa, T. Dauxois, and S. Ruffo, *Phys. Rep.* **480**, 57 (2009).
[8] A. Campa, T. Dauxois, D. Fanelli, and S. Ruffo, *Physics of Long-Range Interacting Systems* (Oxford University Press, Oxford, UK, 2014).
[9] V. A. Antonov, *Vest. Leningr. Gos. Univ.* **7**, 135 (1962).
[10] V. A. Ambarzumian, *Ann. Leningrad State Univ.* **22**, 19 (1938).
[11] L. Spitzer, *Mon. Not. R. Astron. Soc.* **100**, 396 (1940).
[12] S. Chandrasekhar, *Principles of Stellar Dynamics* (University of Chicago Press, Chicago, IL, 1942).
[13] K. F. Ogorodnikov, *Sov. Astron.* **1**, 748 (1957).
[14] K. F. Ogorodnikov, *Sov. Astron.* **1**, 787 (1957).
[15] D. Lynden-Bell and R. Wood, *Mon. Not. R. Astron. Soc.* **138**, 495 (1968).
[16] D. Lynden-Bell, *Extrait du Bulletin Astronomique* **3**, 305 (1968).
[17] M. Hénon, *Ann. Astrophys.* **24**, 369 (1961).
[18] H. Cohn, *Astrophys. J.* **242**, 765 (1980).
[19] G. G. Kuzmin, *Tartu Astr. Obs. Publ.* **33**, 75 (1957).
[20] R. B. Larson, *Mon. Not. R. Astron. Soc.* **147**, 323 (1970).
[21] I. Hachisu, Y. Nakada, K. Nomoto, and D. Sugimoto, *Prog. Theor. Phys.* **60**, 393 (1978).
[22] D. Lynden-Bell and P. P. Eggleton, *Mon. Not. R. Astron. Soc.* **191**, 483 (1980).
[23] S. Inagaki and D. Lynden-Bell, *Mon. Not. R. Astron. Soc.* **205**, 913 (1983).
[24] D. C. Heggie and D. Stevenson, *Mon. Not. R. Astron. Soc.* **230**, 223 (1988).
[25] D. Sugimoto and E. Bettwieser, *Mon. Not. R. Astron. Soc.* **204**, 19P (1983).
[26] P. H. Chavanis, *Astron. Astrophys.* **432**, 117 (2005).
[27] J. Binney and S. Tremaine, *Galactic Dynamics*, Princeton Series in Astrophysics (Princeton University Press, Princeton, NJ, 1987).
[28] R. W. Michie, *Mon. Not. R. Astron. Soc.* **125**, 127 (1962).
[29] I. R. King, *Astron. J.* **70**, 376 (1965).
[30] J. Katz, *Mon. Not. R. Astron. Soc.* **190**, 497 (1980).
[31] P. H. Chavanis, M. Lemou, and F. Méhats, *Phys. Rev. D* **91**, 063531 (2015).
[32] W. Thirring, *Z. Phys.* **235**, 339 (1970).
[33] D. Lynden-Bell and R. M. Lynden-Bell, *Mon. Not. R. Astron. Soc.* **181**, 405 (1977).
[34] R. Emden, *Gaskugeln* (Teubner Verlag, Leipzig, 1907).
[35] P. H. Chavanis, *Astron. Astrophys.* **381**, 340 (2002).
[36] M. Kiessling, *J. Stat. Phys.* **55**, 203 (1989).
[37] P. H. Chavanis, C. Rosier, and C. Sire, *Phys. Rev. E* **66**, 036105 (2002).
[38] C. Sire and P. H. Chavanis, *Phys. Rev. E* **66**, 046133 (2002).
[39] C. Sire and P. H. Chavanis, *Phys. Rev. E* **69**, 066109 (2004).
[40] P. H. Chavanis, *Astron. Astrophys.* **356**, 1089 (2000).
[41] J. Katz, *Mon. Not. R. Astron. Soc.* **183**, 765 (1978).
[42] H. Poincaré, *Acta Math.* **7**, 259 (1885).
[43] E. B. Aronson and C. J. Hansen, *Astrophys. J.* **177**, 145 (1972).
[44] B. Stahl, M. K. H. Kiessling, and K. Schindler, *Planet. Space Sci.* **43**, 271 (1995).
[45] S. Chandrasekhar, *An Introduction to the Theory of Stellar Structure* (Dover, New York, NY, 1942).
[46] J. R. Oppenheimer and G. M. Volkoff, *Phys. Rev.* **55**, 374 (1939).
[47] S. L. Shapiro and S. A. Teukolsky, *Black Holes, White Dwarfs, and Neutron Stars* (Wiley Interscience, Hoboken, NJ, 1983).

- [48] N. Bilic, F. Munyaneza, G. B. Tupper, and R. D. Viollier, *Prog. Part. Nucl. Phys.* **48**, 291 (2002).
- [49] N. Bilic, G. B. Tupper, and R. D. Viollier, *Lect. Notes Phys.* **616**, 24 (2003).
- [50] H. J. de Vega, P. Salucci, and N. G. Sanchez, *Mon. Not. R. Astron. Soc.* **442**, 2717 (2014).
- [51] R. Ruffini, C. R. Argüelles, and J. A. Rueda, *Mon. Not. R. Astron. Soc.* **451**, 622 (2015).
- [52] P. H. Chavanis, The self-gravitating Fermi gas in Newtonian gravity and general relativity, in *Proceedings of the 16th Marcel Grossman Meeting* (World Scientific, Singapore, 2021), retrieved from [arXiv:2112.02654](https://arxiv.org/abs/2112.02654).
- [53] P. H. Chavanis, *Phys. Rev. D* **106**, 043538 (2022).
- [54] C. R. Argüelles, E. A. Becerra-Vergara, J. A. Rueda, and R. Ruffini, *Universe* **9**, 197 (2023).
- [55] P. H. Chavanis, *Eur. Phys. J. B* **87**, 9 (2014).
- [56] B. Bakhti, D. Boukari, M. Karbach, P. Maass, and G. Müller, *Phys. Rev. E* **97**, 042131 (2018).
- [57] P. Hertel and W. Thirring, *Commun. Math. Phys.* **24**, 22 (1971).
- [58] P. Hertel and W. Thirring, in *Quanten und Felder*, edited by H. P. Dürr (Vieweg, Braunschweig, 1971).
- [59] N. Bilic and R. D. Viollier, *Phys. Lett. B* **408**, 75 (1997).
- [60] P. H. Chavanis, *Phys. Rev. E* **65**, 056123 (2002).
- [61] B. N. Miller and P. Youngkins, *Phys. Rev. Lett.* **81**, 4794 (1998).
- [62] E. Follana and V. Laliene, *Phys. Rev. E* **61**, 6270 (2000).
- [63] V. P. Youngkins and B. N. Miller, *Phys. Rev. E* **62**, 4583 (2000).
- [64] P. H. Chavanis and I. Ispolatov, *Phys. Rev. E* **66**, 036109 (2002).
- [65] C. Destri and H. J. de Vega, *Nucl. Phys. B* **763**, 309 (2007).
- [66] N. Bilic and R. D. Viollier, *Eur. Phys. J. C* **11**, 173 (1999).
- [67] Z. Roupas and P. H. Chavanis, *Classic. Quant. Grav.* **36**, 065001 (2019).
- [68] P. H. Chavanis and G. Alberti, *Phys. Lett. B* **801**, 135155 (2020).
- [69] G. Alberti and P. H. Chavanis, *Eur. Phys. J. B* **93**, 208 (2020).
- [70] P. H. Chavanis, M. Lemou, and F. Méhats, *Phys. Rev. D* **92**, 123527 (2015).
- [71] C. Argüelles, M. I. Díaz, A. Krut, and R. Yunis, *Mon. Not. R. Astron. Soc.* **502**, 4227 (2021).
- [72] J. D. Murray, *Mathematical Biology* (Springer, Berlin, 1991).
- [73] D. Horstmann and M. Lucia, *J. Reine Angew. Math.* **2011**, 83 (2011).
- [74] P. H. Chavanis, M. Ribot, C. Rosier, and C. Sire, *Banach Center Publ.* **66**, 103 (2004).
- [75] J. S. Stodolkiewicz, *Acta Astron.* **13**, 30 (1963).
- [76] J. Ostriker, *Astrophys. J.* **140**, 1056 (1964).
- [77] L. Spitzer, *Astrophys. J.* **95**, 329 (1942).
- [78] G. L. Camm, *Mon. Not. R. Astron. Soc.* **110**, 305 (1950).
- [79] J. Katz and D. Lynden-Bell, *Mon. Not. R. Astron. Soc.* **184**, 709 (1978).
- [80] J. Katz and M. Lecar, *Astrophys. Space Sci.* **68**, 495 (1980).
- [81] J. J. Aly, *Phys. Rev. E* **49**, 3771 (1994).
- [82] J. J. Aly and J. Perez, *Phys. Rev. E* **60**, 5185 (1999).
- [83] P. H. Chavanis, *C. R. Phys.* **7**, 331 (2006).
- [84] M. Kiessling, *J. Stat. Mech.* (2011) P01028.
- [85] P. H. Chavanis, *Physica A* **384**, 392 (2007).
- [86] P. H. Chavanis, *Phys. Rev. E* **69**, 066126 (2004).
- [87] P. H. Chavanis, *Phys. Rev. D* **76**, 023004 (2007).
- [88] M. Kirejczyk, G. Müller, and P. H. Chavanis, *Phys. Rev. E* **106**, 024132 (2022).
- [89] M. Kirejczyk, G. Müller, and P. H. Chavanis, *Phys. Rev. E* **105**, 034145 (2022).
- [90] P. H. Chavanis (unpublished).
- [91] P. H. Chavanis, *Astron. Astrophys.* **556**, A93 (2013).
- [92] K. F. Ogorodnikov, *Dynamics of Stellar Systems* (Pergamon, Oxford, UK, 1965).
- [93] R. Ellis, K. Haven, and B. Turkington, *J. Stat. Phys.* **101**, 999 (2000).
- [94] A. Campa and P. H. Chavanis, *J. Stat. Mech.* (2010) P06001.
- [95] P. H. Chavanis and J. Sommeria, *Mon. Not. R. Astron. Soc.* **296**, 569 (1998).
- [96] I. Ispolatov and M. Karttunen, *Phys. Rev. E* **68**, 036117 (2003).
- [97] R. Ruffini and L. Stella, *Astron. Astrophys.* **119**, 35 (1983).
- [98] P. H. Chavanis, *Mon. Not. R. Astron. Soc.* **300**, 981 (1998).
- [99] S. R. Bonsor, A. L. Varri, and J. Vanneste (unpublished).
- [100] J. Sopik, C. Sire, and P. H. Chavanis, *Phys. Rev. E* **72**, 026105 (2005).
- [101] P. H. Chavanis and C. Sire, *Physica A* **384**, 199 (2007).
- [102] C. Sire and P. H. Chavanis, *Phys. Rev. E* **78**, 061111 (2008).
- [103] P. H. Chavanis and C. Sire, *Physica A* **387**, 4033 (2008).
- [104] P. H. Chavanis, *Commun. Nonlinear Sci. Numer. Simulat.* **15**, 60 (2010).
- [105] P. H. Chavanis and L. Delfini, *Phys. Rev. E* **89**, 032139 (2014).
- [106] E. Keller and L. A. Segel, *J. Theor. Biol.* **26**, 399 (1970).
- [107] P. H. Chavanis, *Eur. Phys. J. Plus* **132**, 248 (2017).
- [108] P. H. Chavanis, *Eur. Phys. J. Plus* **134**, 352 (2019).
- [109] J. H. Jeans, *Mon. Not. R. Astron. Soc.* **76**, 70 (1915).